

## ABSTRACT

Title of dissertation: Self-Assembled Photoresponsive and Thermoresponsive Nanostructures

Kunshan Sun, Doctor of Philosophy, 2009

Dissertation directed by: Professor Srinivasa R. Raghavan, Department of Chemical and Biomolecular Engineering

Responsive complex fluids based on nanostructures (e.g., micelles, vesicles and nanoparticles) have received considerable attention recently. The ability of these materials to be tuned by light or heat can have many potential applications in the areas of drug delivery, coatings, sensors, or microfluidic valves and dampers. However, most current photoresponsive and thermoresponsive formulations require the synthesis of complex organic molecules, and this prevents them from being used widely for commercial applications. In this dissertation, we seek to develop new classes of photoresponsive (PR) and thermoresponsive (TR) nanostructures based on commercially available, inexpensive precursors.

In the first part of this study, we report a new PR fluid based on light-activated nanoparticle assembly. Our system consists of disk-like nanoparticles of laponite along with a surfactant stabilizer (Pluronic F127) and the photoacid generator (PAG), diphenyliodonium-2-carboxylate monohydrate. Initially, the nanoparticles are sterically stabilized by the surfactant and the result is a stable, low-viscosity dispersion. Upon UV irradiation, the PAG gets photolyzed, lowering the pH by about 3 units. In turn, the

stabilizing surfactant is displaced from the negatively charged faces of the nanoparticle disks while the edges of the disks become positively charged. The particles are thereby induced to assemble into a 3-dimensional “house-of-cards” network that extends through the sample volume. The net result is a light-induced *sol to gel transition*, i.e., from a low, water-like viscosity to an *infinite* viscosity and yield stress. The yield stress of the photogel is sufficiently high to support the weight of small objects. The gel can be converted back to a sol by either increasing the pH or the surfactant content. Evidence for the above mechanism is provided from a variety of techniques, including small-angle neutron scattering (SANS).

In the second part of this study, we demonstrate that laponite/PF127 mixtures also show thermogelling, i.e., the fluids transform from low viscosity sols to stiff gels upon heating above a critical temperature. This phenomenon is reversible and it requires the presence of sufficient amounts of both components. At room temperature, PF127 adsorbs onto laponite disks and stabilizes them by steric repulsion. Upon heating, the PF127 layer on the disks becomes thicker, and more importantly, PF127 micelles in the bulk solution grow significantly. Evidence for the growth of micelles is presented from SANS modeling and from transmission electron microscopy (TEM). At a distinct temperature, we believe the micelles induce *depletion flocculation* of the laponite particles into a gel network. Interestingly, if the PF127 concentration is increased further, the thermogelling is eliminated – this is suggested to be due to the micelles providing *depletion stabilization* of the particles.

# SELF-ASSEMBLED PHOTORESPONSIVE AND THERMORESPONSIVE NANOSTRUCTURES

Kunshan Sun

Dissertation submitted to the Faculty of the Graduate School of the  
University of Maryland, College Park, in partial fulfillment  
of the requirements for the degree of  
Doctor of Philosophy  
2009

Advisory Committee:

Professor Srinivasa R. Raghavan, Chair

Professor Sheryl Ehrman

Professor Jeffery B. Klauda

Professor Daniel Falvey

Professor Bruce Yu

© Copyright by  
Kunshan Sun  
2009

## Acknowledgements

First of all, I would like to thank my advisor Dr. Srinivasa Raghavan. Without his encouragement, advice and tolerance, I can't find my own way of doing research. His writing and presentation skills, research philosophy, training and guidance style worth my study before, now and in the future. I feel lucky to join his group.

I would like to thank my wife Lingling for her support all along my way of research. There are highs and lows in the life, and you share my happiness and give me strength. With you, I never feel lonely. I would also like to thank my little baby Handong (Franklin). Your smile face can get rid of any grey corner of my heart.

I would also like to thank my committee: Dr. Ehrman, Dr. Klauda, Dr. Falvey and Dr. Yu. Thank you for your advice and suggestions. I'm grateful to undergraduate students who have worked with me, Nick Harrigen and Alex Marhefka. Thank you for your effort put in the research. Additionally, I would like to acknowledge Li-Chung Lai for his assistance in TEM experiments.

I am grateful to all of my group colleagues who have shared happy research life in Dr. Raghavan's lab: Shihuang Tung, Bani Cipriano, Aimee Ketner, Hee-Young Lee, Rakesh Kumar, Matt Dowling, Chao Zhu, Oluwatosin Ogunsola, Peter Thomas, George Chacko, Khyati Tiwari, Vishal Javvaji, Veidhes Basrur, Kunqiang Jiang and Charles Kuo.

We are such a large family and we have a lot of fun in discussions and out of lab activities. I would also like to thank my friends here who have helped and supported me.

Finally, I would like to acknowledge NIST for facilitating the SANS experiments. This work was partially funded by NSF CAREER Award and Dr. Jane Emerson's lab in Southern California University.

# TABLE OF CONTENTS

Acknowledgements .....	ii
Table of Contents .....	iv
List of Tables .....	vi
List of Figures .....	vii
Chapter 1: Introduction and Overview .....	1
1.1. Problem Description and Motivation.....	1
1.2. Our Approach .....	2
Chapter 2: Background .....	5
2.1. Laponite and its Aqueous Gels .....	5
2.2. Pluronic Copolymers.....	8
2.3. Photoacid Generators .....	9
2.4. Characterization Technique – I: Rheology .....	9
2.5. Characterization Technique – II: SANS.....	11
2.6. Characterization Technique – III: DLS .....	13
Chapter 3: Photogelling Behavior of Nanoparticle Dispersions .....	15
3.1. Introduction .....	15
3.2. Experimental Section .....	19
3.3. Results and Discussion .....	24
3.4. Conclusions .....	36

Chapter 4: Reversible Thermogelling of Nanoparticle Dispersions .....	37
4.1. Introduction .....	37
4.2. Experimental Section .....	39
4.3. Results and Discussion .....	41
4.4. Conclusions .....	53
Chapter 5: Conclusions and Recommendations.....	54
5.1. Conclusions .....	54
5.2. Recommendations for Future Work .....	56
Chapter 6: References .....	58



## LIST OF TABLES

<b>Table 3.1.</b> Key parameters of SANS modeling for 1.4% laponite + 1.7% PF127 + 13 mM PAG before and after 15 min UV irradiation.	30
<b>Table 4.1.</b> Key parameters of SANS modeling for 0.5% laponite + 0.6% PF127 and 1.4% laponite + 1.7% PF127 at 25°C and 80°C.	48

## LIST OF FIGURES

- Figure 1.1.** Photogelling fluid described in Chapter 3 based on a mixture of laponite nanoparticles, the amphiphilic polymer, PF127 and a photoacid generator, PAG. Initially (a), the particles are unconnected and the system is a low viscosity fluid. After UV irradiation (b), the particles assemble into a 3-D network, and accordingly the sample becomes a stiff gel that can hold its weight in the inverted vial. 2
- Figure 2.1.** (a) Schematic of a single laponite nanoparticle. (b) The origin of permanent negative charge on these particles. 5
- Figure 2.2.** Source of negative charges on the surfaces and edges of laponite platelets. 6
- Figure 2.3.** Schematic of a card-house gel formed by laponite particles in water. 7
- Figure 2.4.** Molecular structure and composition grid for Pluronic® copolymers. 8
- Figure 2.5.** Schematic of a SANS experiment (adapted from [www.gkss.de](http://www.gkss.de)). 12
- Figure 3.1.** The three components of the photorheological (PR) fluids described in this paper. (a) laponite nanoparticles; (b) the triblock copolymer, Pluronic F127 (PF127); and (c) the photoacid generator (PAG), diphenyliodonium-2-carboxylate monohydrate. Upon UV irradiation, the PAG gets photolysed into benzoic acid and iodobenzene. 17
- Figure 3.2.** Photogelling of a 3% laponite + 3.6% PF127 + 13 mM PAG sample. Initially (a), the sample is a low-viscosity fluid: the particles are unconnected and stabilized by the adsorbed PF127. Upon UV irradiation (b), the particles assemble into a “card-house” network, causing the fluid to gel. In this case, the PF127 no longer covers the particle surface; instead it forms discrete micelles in solution. Note that the photogel holds its weight in the inverted vial and the stirrer bar is trapped in it. 24
- Figure 3.3.** Dynamic rheology of a 1.4% laponite + 1.7% PF127 + 13 mM PAG sample (a) before and (b) after 15 minutes of UV irradiation. Before UV irradiation, the sample shows a purely viscous response, characteristic of a liquid. After irradiation, the sample response is purely elastic and characteristic of a gel. The gel modulus is about 300 Pa. 25
- Figure 3.4.** Steady-shear rheology of a 3% Laponite + 3.6% PF127 + 13 mM PAG sample before and after UV irradiation for various periods of time. The sample switches from a low-viscosity, Newtonian fluid to a strong gel with progressive irradiation. The final gel has a yield stress of ~ 30 Pa, which is sufficient to hold the weight of a pen. 26

**Figure 3.5.** (a) Effect of PAG concentration on photogelling. Steady-shear data are shown for samples containing 1.4% laponite + 1.7% PF127 + various amounts of PAG before and after 15 min of UV irradiation. (b) Effect of laponite concentration on photogelling. Steady-shear data before and after UV irradiation for 20 min are shown for samples containing 13 mM PAG with various amount of laponite + PF127. In both cases, data before UV are shown using unfilled symbols and after UV with filled symbols. 27

**Figure 3.6.** SANS scattering spectra (intensity  $I$  vs. wave-vector  $q$ ) for samples containing 1.4% laponite + 1.7% PF127 and with three different PAG concentrations. Data before UV irradiation are shown as red symbols and that after 15 min of UV irradiation are shown as violet symbols. For the 13 mM PAG sample, the data before and after UV are fit to models as described in the text, and the model fits are shown as solid lines. 29

**Figure 3.7.** Mechanism for photogelling. Initially, laponite disks are stabilized by PF127, with the hydrophobic PPO portion (red segment) of PF127 adsorbed on the particles and the hydrophilic PEO portions (blue) extending into water. Upon UV irradiation, the PAG splits into benzoic acid and iodobenzene. The PF127 desorbs from the laponite and forms micelles in solution, taking up the hydrophobic iodobenzene. The lowering of pH by the benzoic acid causes the particle edges to turn positive. In turn, the particles assemble into a network due to interactions between the positive edges and the negative faces. 32

**Figure 3.8.** Schematics of experiments that give insight into the photogelling mechanism. (a) A sol of laponite+PF127 can be gelled if both iodobenzene and benzoic acid are added, but not if only one of the two are added. (b) A gel of laponite+PF127+PAG can be liquefied (ungelled) by either adding more PF127 or by increasing the pH. The former can be gelled again by adding more iodobenzene. The sols are also temperature sensitive and can be gelled by heating to 70° C. 35

**Figure 4.1.** Thermogelling of a 3% laponite + 3.6% PF127 sample, both in its neat form as well as in conjunction with 40% of TiO<sub>2</sub> pigment particles. At room temperature or 25°C (a), the samples are low-viscosity, freely flowing fluids. At 70°C (b), both samples are transformed into gels. Note that the thermogels hold their weight in the inverted vials, indicating substantial yield stresses. 41

**Figure 4.2.** Dynamic rheology of a 3% laponite + 3.6% PF127 sample at (a) 25°C and (b) 70°C. At 25°C, the sample shows a viscous response, characteristic of a liquid. At 70°C, the sample response is elastic and characteristic of a gel. 43

**Figure 4.3.** Steady-shear rheology of a 3% Laponite + 3.6% PF127 sample at different temperatures. Around 65°C, the sample abruptly transforms from a low-viscosity, Newtonian fluid to a gel-like sample having a yield stress (marked by arrows). 43

**Figure 4.4.** Effect of laponite concentration on thermogelling. Steady-shear data at 25°C and high temperatures are shown for samples containing 1.7% PF127 and varying amounts of laponite. Data at 25°C are shown using unfilled symbols and those at high temperatures are shown with filled symbols. Thermogelling occurs only for laponite concentrations above a minimum value. 45

**Figure 4.5.** Effect of PF127 concentration on thermogelling. Steady-shear data are shown for samples containing 1.4% laponite and varying amounts of PF127 at 25°C and high temperatures. Thermogelling occurs only at intermediate PF127 concentrations (panel B); it does not occur either at lower or higher concentrations of PF127. 46

**Figure 4.6.** SANS scattering spectra (intensity  $I$  vs. wave-vector  $q$ ) at 25 and 80°C for samples containing (a) 0.5% laponite + 0.6% PF127 and (b) 1.4% laponite + 1.7% PF127. The data are fit to models (see text), and the model fits are shown as solid lines. 47

**Figure 4.7.** TEM images corresponding to a 0.5% laponite + 0.6% PF127 sample at 25°C (left) and 80°C (right). The images are stained with uranyl acetate. The image on the right shows a large number of PF127 micelles. 50

**Figure 5.1.** Photolysis of MGC, a photobase generator (PBG). Upon UV irradiation, the molecule dissociates and releases  $\text{OH}^-$ . After UV, it will automatically reverse back. 56

**Figure 5.2.** UV response of 100mM lecithin+600mM water+0.48mM MGC in cyclohexane. Pictures are taken 1 second after inverting the vials. 57

# Chapter 1

## Introduction and Overview

---

### 1.1 Problem Description and Motivation

Recently, there has been considerable interest in complex fluids that can be controlled by external stimuli such as heat, pH, electric fields, magnetic fields, and light. Responsive systems may be useful in applications such as drug delivery, wound healing, cancer therapy, sensors, microfluidics or MEMS devices, paints, coatings, personal care products, and traditional mechanical engineering applications like dampers, shock absorbers, and brakes<sup>1-7</sup>. Light is a special stimuli which can be directed at a specific point with resolution of a few microns or less. Thus, light-responsive fluids (PR fluids) may be particularly suited for microscale or nanoscale applications, such as in microfluidic devices. Thermo-responsive fluids (TR fluids), on the other hand, will be particularly suited for heat-related applications, such as baking paints, coatings, personal care products and fire fighting agents.

Currently, light-responsive formulations have been developed in the lab, but these have not translated into a wide range of commercial applications yet. The underlying reason for this is that most light-responsive materials are based on complex organic molecules,<sup>6-9</sup> which have to be synthesized and purified by elaborate procedures. Even in the case of thermo-responsive fluids, complex molecules requiring synthesis are often used. Organic synthesis can be both labor-intensive and costly, which is often a deterrent

to widespread investigation in research labs, both industrial and academic. So our motivation here is to make light-responsive and thermo-responsive fluids based on inexpensive commercially available materials, and thus our work could open up the study of PR and TR fluids to many more academic and industrial researchers.

## 1.2 Our Approach

In this dissertation, we are interested in developing new classes of photoresponsive and thermoresponsive systems based on commercially available, inexpensive molecules and particles.

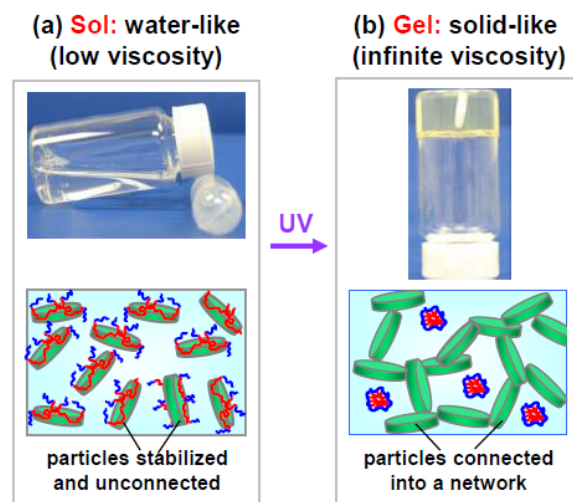


**Figure 1.1.** Photogelling fluid described in Chapter 3 based on a mixture of laponite nanoparticles, the amphiphilic polymer, PF127 and a photoacid generator, PAG. Initially (a), the particles are unconnected and the system is a low viscosity fluid. After UV irradiation (b), the particles assemble into a 3-D network, and accordingly the sample becomes a stiff gel that can hold its weight in the inverted vial.

In Chapter 3, we describe the photoresponsive system depicted in Figure 1.1. This is a photorheological (PR) fluid, i.e., one that undergoes changes in its rheological or

flow properties (such as viscosity) upon irradiation with light. The concept underlying this class of PR fluids is light-activated assembly of a type of nanoparticles called laponite. Initially (before irradiation), as shown in Figure 1.1(a), the sample is a low-viscosity aqueous fluid that flows easily upon tilting the vial. In this state, the laponite nanoparticles, shown as disks, are unconnected and form a stable dispersion. Upon UV irradiation, the nanoparticles are induced to assemble into a 3-dimensional (3-D) volume-filling network, as shown in Figure 1.1(b). In turn, the sample is transformed into a gel of infinite viscosity and appreciable yield stress ( $\sim 30$  Pa) – this is indicated by the fact that the gel holds its weight in the vial. The mechanism behind the PR effect in this fluid will be discussed in Chapter 3; note that the other components in the system are a photo-acid generator (PAG) and an amphiphilic polymer, Pluronic F127 (PF127).

It is useful to contrast the above PR fluid with those developed previously in our lab and elsewhere. Firstly, as mentioned previously, PR fluids developed by others tend to rely on new organic molecules such as photoresponsive surfactants or polymers containing azobenzene units that have to be synthesized specifically for this purpose.<sup>6-9</sup> In contrast, the three components of our PR fluid (laponite, PF127, PAG) are all commercially available and quite inexpensive. Thus, it is easy for other researchers to replicate our results and focus on finding applications for these fluids. Simple, low-cost approaches to PR fluids have been a point of emphasis in our lab and we have previously reported two such systems, one a photothinning one<sup>10</sup> and the other a photogelling one<sup>11</sup>. Both are based on commercial surfactants and organic acids, and in both cases, the PR effect was due to light-induced changes in the length of surfactant aggregates called

“wormlike micelles”. However, while significant changes in viscosity were reported, the high-viscosity state in those systems were not “true” gels, i.e., they did not have a finite yield stress. In the present case, we are able to achieve a true sol-to-gel transition (Figure 1.1b), which is thus an improvement over earlier work from our lab. Moreover, the PR effect in our case is due to nanoparticle assembly, not transitions in the sizes of micellar structures – i.e., an entirely different concept.

During our work with the above photoresponsive nanoparticle system, interestingly enough we found that similar systems (mixtures of laponite and PF127) are also thermo-responsive. That is, the initial low-viscosity sols gelled upon heating to about 60°C and the gels reverted to sols upon cooling. We will probe the underlying mechanism for such thermogelling of these nanoparticle dispersions in Chapter 4. As we shall see, the responsiveness again comes from the self-assembly of the nanoparticles, but the causes for nanoparticle assembly are very different.

The significance of this work is in the development of new stimuli-responsive nanostructured materials that do not have the limitations inherent in existing systems. We hope that the availability of simple and elegant stimuli-responsive formulations, based on commercially available nanoparticles and amphiphiles, will prove beneficial to researchers, both in academia and industry. The new directions we have set forth in this thesis will hopefully be explored further by other researchers, and we hope that it will eventually culminate in practical applications for stimu-responsive systems in both existing as well as emerging technologies.



## Chapter 2

### Background

---

This dissertation is concerned with photoresponsive and thermoresponsive nanostructures. In this chapter, we will discuss the basics of laponite nanoparticles and certain photoresponsive molecules. We then describe the techniques that we will use to study these types of structures, such as rheology, small-angle neutron scattering (SANS), and dynamic light scattering (DLS).

#### 2.1. Laponite and its Aqueous Gels

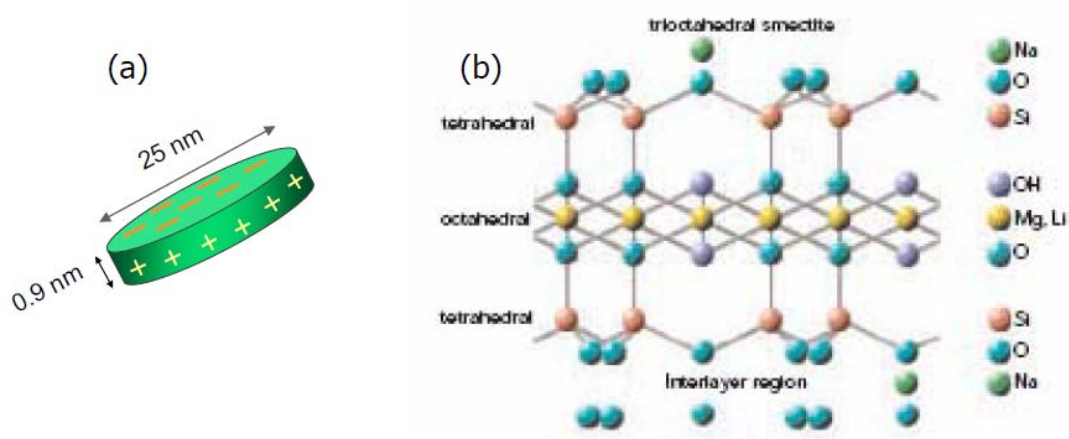


**Figure 2.1.** (a) Schematic of a single laponite nanoparticle. (b) The origin of permanent negative charge on these particles.<sup>12</sup>

Laponite is a synthetic clay that exists as disklike nanoparticles with a diameter of 25 nm diameter and a thickness of 0.92 nm (Figure 2.1a).<sup>12</sup> The “ideal” laponite

composition is  $\text{H}_2\text{Si}_4\text{Mg}_3\text{O}_{12}$ , which results in an “ideal” net charge of  $[2(+2)+4(+4)+2(+3)+12(-2)] = 0$ . However, the real composition involves isomorphous substitution of  $\text{Li}^+$  for some  $\text{Mg}^{2+}$  in the octahedral sheet (Figure 2.1b). Due to this substitution, there are fewer positive charges to neutralize the negative charges and a large permanent negative charge results on the face of the disks at all pH (see also Figure 2.2).<sup>13</sup> The edges of the platelets, in contrast, have a charge that is pH dependent due to the presence of amphoteric groups: Mg-OH, Li-OH and Si-OH. These surface groups can be protonated or deprotonated depending on the pH of the surrounding solution. While Mg-OH and Li-OH are positively charged below pH 9, Si-OH (silanol) groups are negatively charged. Thus, below pH 9, the edges of laponite platelets are positively charged while above pH 9 the edges are negatively charged.<sup>14,15</sup>

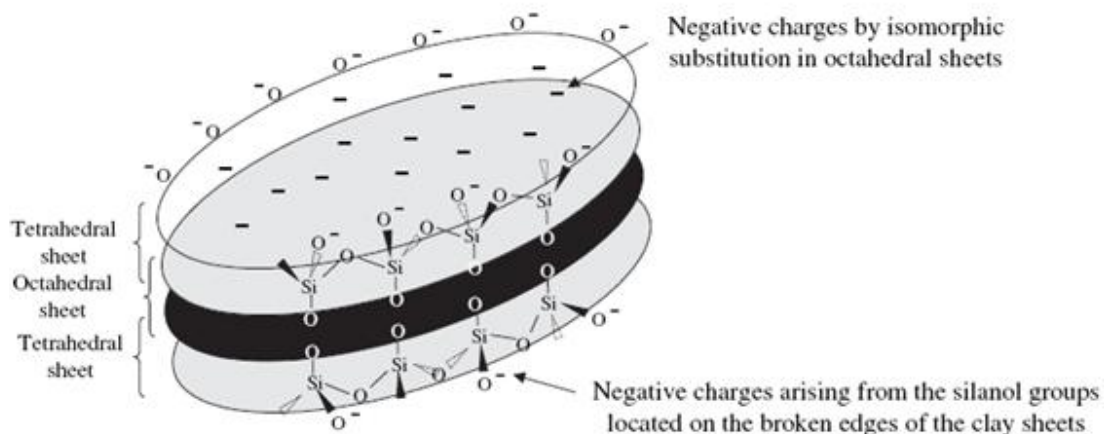


**Figure 2.2.** Source of negative charges on the surfaces and edges of laponite platelets.<sup>13</sup>

When laponite particles are added to water at concentrations exceeding ca. 3 wt%, they can form gels in two different ways. First, at a pH lower than 9, laponite forms an

interconnected card-house (or “house of cards”) structure, which is similar to a 3-D flocculated network formed by other particles. This causes the aqueous dispersion to become a stiff, elastic gel. Incidentally, all dispersions of laponite start out as low-viscosity liquids but the card-house gel is formed upon aging for about 24 h. The mechanism behind the card-house structure is believed to be the electrostatic interactions between the negatively charged platelet faces and the positively charged platelet edges, as shown in Figure 2.3.

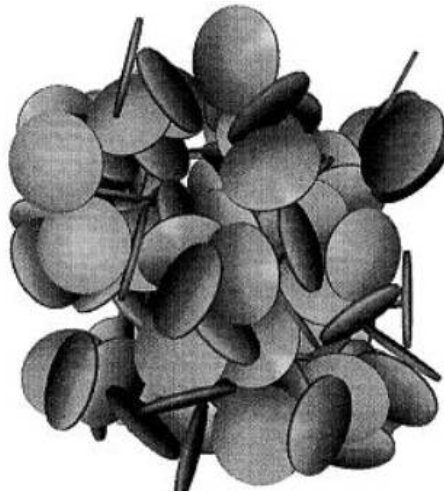


**Figure 2.3.** Schematic of a card-house gel formed by laponite particles in water.<sup>16</sup>

At pH higher than 9, aqueous dispersions of laponite will age into “repulsion gels” due to strong electrostatic repulsions between the particles. Note that at these pH, the entire particle has a strong negative charge. If this charge is unscreened, i.e., at low salt concentrations, the electrostatic double layers surrounding the particles will overlap, and these overlapping shells will pervade the volume. This is believed to give rise to the repulsion gels.

## 2.2. Pluronic Copolymers

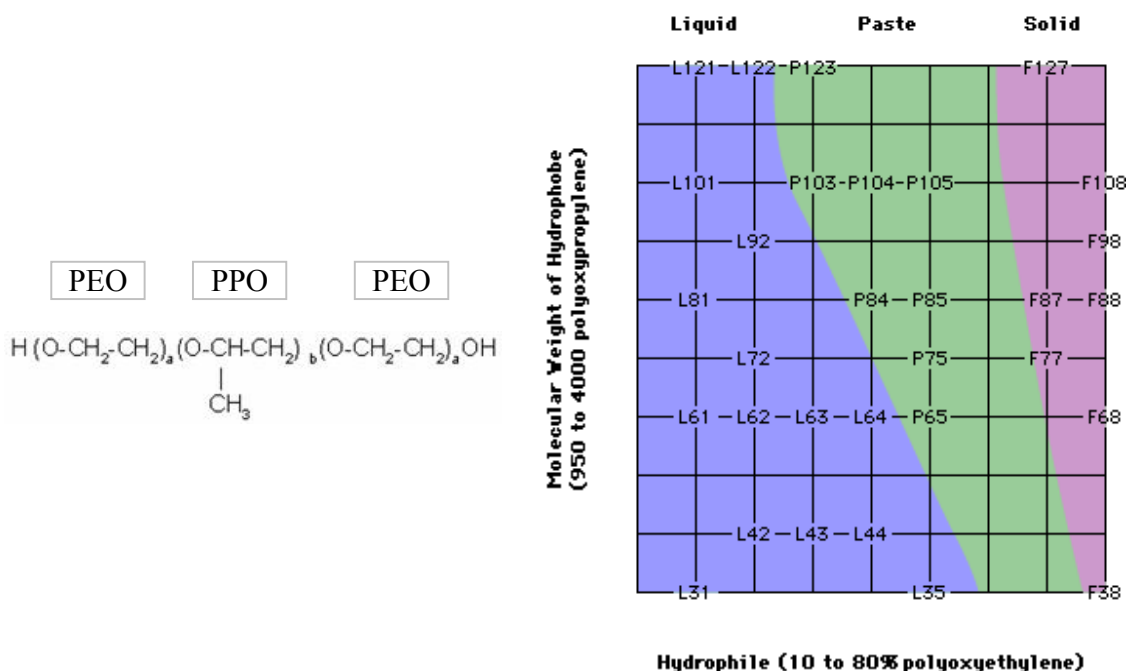


**Figure 2.4.** Molecular structure and composition grid for Pluronic® copolymers.<sup>16</sup>

Pluronic® refers to a class of triblock copolymers of the form PEO-PPO-PEO, where PEO stands for polyethylene oxide and PPO refers to polypropylene oxide (Figure 2.4). Among the two, PEO is relatively hydrophilic and PPO is hydrophobic. Thus, Pluronic copolymers have amphiphilic properties and are popular in industry as formulation aids. The Pluronic grid (Figure 2.4) is a graphic presentation of the series of available copolymer products: it plots the molecular weight of the hydrophobe (PPO) against the wt% of the hydrophile (PEO). The grid also clarifies the use of letter-number combinations to identify products of the series. The alphabetical designation explains the physical form of the product: ‘L’ for liquids, ‘P’ for pastes, ‘F’ for solid forms. The first digit (two digits in a 3-digit number) in the numerical designation, multiplied by 300, indicates the approximate molecular weight of the PPO segment. The last digit, when

multiplied by 10, indicates the approximate PEO content in the molecule. Taking the example of Pluronic F127 (PF127), the molecular weight of its PPO is ~ 3600 (12 x 300) and the wt% of PEO is ~ 70% (7 x 10). When these polymers are combined with particles such as laponite, the hydrophobic PPO segment adsorbs on the laponite surface while the hydrophilic PEO segments extend into the aqueous phase.<sup>17</sup> As a result, the PEO segments will impart steric stability to the particles. This is indeed the case with laponite, as we shall see in Chapter 3 – neither the card-house gel nor the repulsion gel of laponite forms when PF127 is added to the water.<sup>18</sup>

### **2.3. Photoacid Generators**

Photoacid generators (PAGs) are organic molecules that can generate acid moieties upon irradiation at certain wavelengths of light. In Chapter 3, we have used diphenyliodonium-2-carboxylate monohydrate, a PAG that has a relatively high solubility in water. When this PAG is irradiated with UV light, it dissociates into benzoic acid and iodobenzene (see Figure 3.1 in Chapter 3).<sup>19</sup> Note that one of these compounds is polar with a carboxylate (COOH) group while the other is hydrophobic. The ionization of the carboxylate releases H<sup>+</sup> ions, meaning a reduction in solution pH.

### **2.4. Characterization Technique – I: Rheology**

Rheology is formally defined as the study of deformation and flow in materials.<sup>20</sup> Rheological measurements are useful in characterizing complex fluids and they help to correlate the microstructure to the macroscopic flow properties of the material.<sup>21</sup> These measurements are typically performed under steady or dynamic shear. In the case of

steady shear, the sample is subjected to a constant shear-rate  $\dot{\gamma}$  and the response is measured as a shear-stress  $\sigma$ . The ratio of shear stress to shear rate is the (apparent) viscosity  $\eta$ . A plot of  $\eta$  vs. shear rate is called the flow curve of the material. Several fluids show a Newtonian behavior in their flow curve at low shear rates i.e., in this regime, the viscosity is *independent* of shear rate. The viscosity in this region is the zero-shear viscosity  $\eta_0$ , and it corresponds to the viscosity in the limit of  $\dot{\gamma} \rightarrow 0$ .<sup>22</sup>

Rheological experiments can also be conducted in dynamic or oscillatory shear, where a sinusoidal strain  $\gamma = \gamma_0 \sin(\omega t)$  is applied to the sample. Here  $\gamma_0$  is the strain-amplitude (i.e. the maximum applied deformation) and  $\omega$  is the frequency of the oscillations. The sample response will be in the form of a sinusoidal stress  $\sigma = \sigma_0 \sin(\omega t + \delta)$ , which is shifted by a phase angle  $\delta$  relative to the strain waveform. The stress can be decomposed into two components using trigonometric identities, the first in-phase with the sinusoidal strain, and the second out-of-phase by  $90^\circ$ :

$$\sigma = \gamma_0 [G'(\omega) \sin(\omega t) + G''(\omega) \cos(\omega t)] \quad (2.1)$$

where  $G'$  is the Elastic or Storage Modulus and  $G''$  is the Viscous or Loss Modulus. The dynamic experiment ultimately yields plots of  $G'$  and  $G''$  as functions of  $\omega$  (usually plotted on a double-log scale), which are collectively called the frequency spectrum of the material. Such a plot is important because it shows how the viscoelasticity of the material varies with timescale, which in turn is a signature of the microstructure.<sup>20</sup>

The physical interpretation of  $G'$  and  $G''$  are as follows. The elastic modulus  $G'$  is obtained from the in-phase component of the stress and provides information about the elastic nature of the material. Since elastic behavior implies the storage of deformational energy,  $G'$  is also called the storage modulus. The viscous modulus  $G''$ , on the other hand, is the out-of-phase component of the stress, and it characterizes the viscous nature of the material. Since viscous deformation results in the dissipation of energy,  $G''$  is also known as the loss modulus. For  $G'$  and  $G''$  to be meaningful, the dynamic experiments are done in the “linear viscoelastic” or LVE regime,<sup>22</sup> which means the stress is linearly related to the strain. In that case,  $G'$  and  $G''$  will be independent of strain amplitude and will be functions only of the frequency  $\omega$  – the moduli will then be true material properties.

An important advantage of dynamic rheology is that it enables the characterization of a material without disrupting its structure in the process. The net deformation on the sample is minimal, because only small-amplitude strains are used (within the LVE regime). As a result, the linear viscoelastic moduli reflect the microstructure in the sample at rest.<sup>20</sup> In contrast, steady-shear rheology measures material properties under flow conditions, which means relatively large deformations. We can therefore correlate dynamic rheological parameters to static microstructures and steady-shear measurements to flow-induced changes in the microstructure.

## **2.5. Characterization Technique – II: SANS**

Scattering techniques are invaluable probes of micro- and nanostructure in materials<sup>23</sup>. Their basic principle is that the intensity of scattered radiation from a

structured fluid is a function of the size, shape, and interactions of the “particles” present. Small-angle neutron scattering (SANS) is the technique of choice in studying our samples as it probes structure over size scales  $\sim$  a few nm. In SANS, the contrast between the solvent and the “particles” is achieved by switching the hydrogen in the solvent with deuterium, e.g., using  $D_2O$  instead of  $H_2O$ . SANS requires a nuclear reactor to generate neutrons and we are fortunate to have one of the premier SANS facilities nearby at the National Institute of Standards and Technology (NIST) in Gaithersburg, MD.

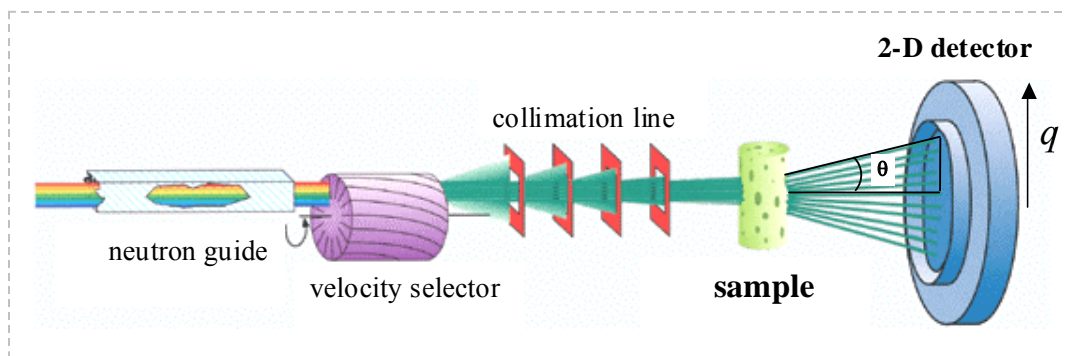


**Figure 2.5.** Schematic of a SANS experiment (adapted from [www.gkss.de](http://www.gkss.de)).

The basic geometry of a SANS experiment is shown in Figure 2.8. Neutrons from a nuclear reactor pass through a velocity selector set for a particular wavelength and wavelength spread. These neutrons then pass through several collimating lenses and into the sample placed in the sample chamber. The neutrons scattered by the sample are collected on a 2-D detector. Using calibration standards, this 2-D data is corrected and placed on an absolute scale. It is then converted into a plot of scattered intensity  $I$  vs. wave vector  $q$  by spherical averaging. The wave vector is defined as<sup>23</sup>:



$$q = \frac{4\pi}{\lambda} \sin\left(\frac{\theta}{2}\right) \quad (2.2)$$

Here,  $\lambda$  is the wavelength of the incident radiation and  $\theta$  is the scattering angle. Thus,  $q$  can be considered an inverse length scale, with high  $q$  corresponding to small structures, and vice versa.

## 2.6 Characterization Technique – III: DLS

Static scattering techniques such as SANS provide information about the quiescent structure. Dynamic scattering techniques have a complementary role in that they probe structural relaxations and dynamics. In particular, dynamic light scattering (DLS) probes the Brownian motion of particles in a fluid. This method can give a reliable estimate of particle size under certain limiting conditions. In a DLS experiment, the fluctuating intensity of light scattered from the sample is recorded at a certain angle  $\theta$ . The fluctuations are then analyzed to yield the intensity autocorrelation function  $g^{(2)}(q, \tau)$  as a function of the correlation time  $\tau$ :<sup>24</sup>

$$g^{(2)}(q, \tau) = \frac{\langle I(q, t)I(q, t + \tau) \rangle}{\langle I(q, t)^2 \rangle} \quad (2.3)$$

Note that in light scattering, the definition of the scattering vector is slightly modified as:

$$q = \frac{4\pi n}{\lambda} \sin\left(\frac{\theta}{2}\right) \quad (2.4)$$

where  $n$  is the refractive index of the medium (the wavelength of light through the medium is thus  $\lambda/n$ ). Thus, in DLS, relaxation is measured at length scales of  $q^{-1}$ .

The measured intensity autocorrelation function  $g^{(2)}(q, \tau)$  can be converted into an electric field autocorrelation function  $g^{(1)}(q, \tau)$  through the Siegert relation.<sup>24</sup>

$$g^{(2)}(q, \tau) = 1 + f |g^{(1)}(q, \tau)|^2 \quad (2.5)$$

Here,  $f$  is an adjustable parameter called the coherence factor that depends on instrument geometry. For a dilute solution of monodisperse spherical particles,  $g^{(1)}(q, \tau)$  is a single exponential decay determined by the translational diffusion coefficient of the particle  $D$ :

$$g^{(1)}(q, \tau) = \exp(-Dq^2\tau) \quad (2.6)$$

From the measured  $D$ , the particle size can be obtained by the Stokes-Einstein equation:

$$D = \frac{k_B T}{6\pi\eta R_h} \quad (2.7)$$

where  $k_B$  is the Boltzmann constant,  $T$  the absolute temperature and  $\eta$  the viscosity of the solvent (assumed to be a Newtonian liquid). The size obtained from DLS is the *hydrodynamic radius*  $R_h$ , i.e., the bare particle size along with any solvation layer.

## Chapter 3

# Photogelling Behavior of Nanoparticle Dispersions

---

The results presented in this chapter have been published in the following journal article:  
Kunshan Sun, Rakesh Kumar, Daniel E. Falvey and Srinivasa R. Raghavan,  
“*Photogelling colloidal dispersions based on light-activated assembly of nanoparticles.*”  
Journal of the American Chemical Society, 131, 7135-7141 (2009).

### 3.1 Introduction

Numerous research group<sup>6,8-11,25-32</sup> have been interested in creating fluids whose rheological properties, such as viscosity, can be tuned by irradiation with light (for reviews, see<sup>8,26-28</sup>). Such *photorheological* (PR) fluids<sup>10,25</sup> could be particularly attractive for creating microvalves or flow sensors within microfluidic systems. Indeed, compared to other external stimuli such as heat or magnetic fields, light does offer distinct advantages in microscale applications – notably, in its ability to be directed at a precise spot with micron-level resolution. For PR fluids to be used widely, researchers need to be able to create them at will – preferably from inexpensive and commercially available components. However, most of the PR systems developed to-date have been based on complex organic molecules, such as photoresponsive surfactants,<sup>6,8,9</sup> polymers,<sup>28-30</sup> or gelators,<sup>27,31,32</sup> most of which are not commercially available and whose synthesis demands considerable skill in organic chemistry. There is a need for simpler approaches to making PR fluids, and this has been the focus of our work.

Recently, we have demonstrated two sets of PR fluids, a photothinning one<sup>10</sup> and a photogelling one,<sup>11</sup> both of which are based on simple, widely available molecules. Both fluids employ the photoisomerizable organic molecule, *trans*-ortho-methoxycinnamic acid (OMCA). The photothinning fluid combines OMCA with a conventional cationic surfactant.<sup>10</sup> In this case, UV irradiation of the fluid causes a substantial decrease in viscosity (factors of 1000 to 10,000). The photogelling fluid combines OMCA with a zwitterionic surfactant and in this case, the fluid viscosity increases dramatically upon UV irradiation.<sup>11</sup> The mechanisms for the photorheological effects in both systems involve changes in the length of cylindrical (“wormlike”) micelles. When the micelles are short, the viscosity is low; conversely, long micellar chains entangle with each other to give a high viscosity. The micelle length, in turn, is modulated by the binding tendency of the OMCA isomer (*trans* vs. *cis*). In both the above systems, the light-induced viscosity change is not reversible by irradiation with a different wavelength of light, but it is reversible by changing the system composition. Despite this limitation, our studies have shown that significant light-induced rheological changes are indeed possible in very simple systems.

In this paper, we report a new class of PR fluids based on an entirely different concept compared to the one discussed above. The key ingredient in our present fluids are *nanoscale particles* of the synthetic clay, laponite (Figure 3.1a).<sup>12,15,16,33</sup> These particles are initially dispersed in water as individual, unconnected disks, thus forming a low-viscosity fluid. Upon irradiation with UV light, the particles are induced to assemble into a 3-dimensional network that pervades the sample volume. The resulting aqueous gel

has an infinite viscosity and a yield stress. In effect, our system shows a light-induced sol-gel transition, with the gel being held by physical (electrostatic) bonds. The gel can be converted back to a sol by changing the pH, but not by irradiation with a different wavelength of light.

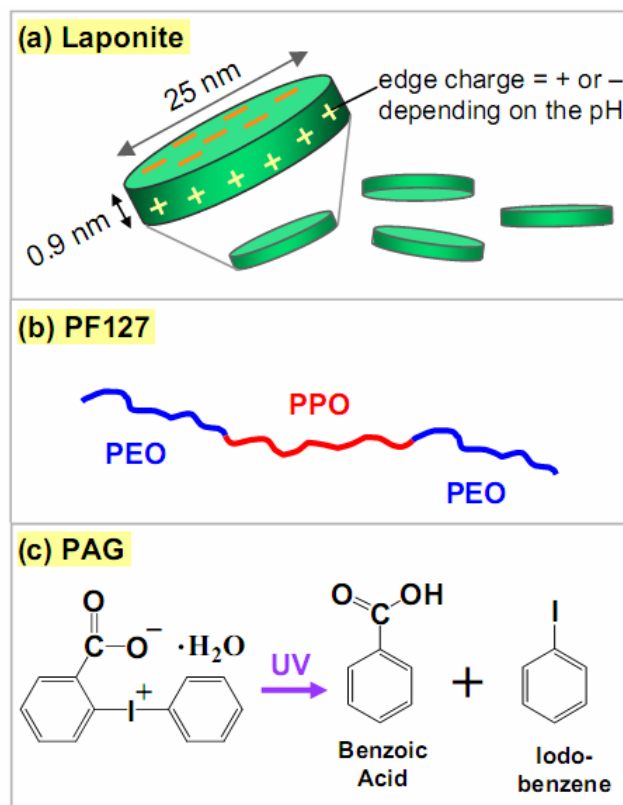


**Figure 3.1.** The three components of the photorheological (PR) fluids described in this paper. (a) laponite nanoparticles; (b) the triblock copolymer, Pluronic F127 (PF127); and (c) the photoacid generator (PAG), diphenyliodonium-2-carboxylate monohydrate. Upon UV irradiation, the PAG gets photolysed into benzoic acid and iodobenzene.

How does this work? In addition to the laponite, the fluids have two other components (Figure 3.1b, 3.1c): the nonionic surfactant, Pluronic F127 (PF127), and the photoacid generator, diphenyliodonium-2-carboxylate monohydrate (abbreviated as

‘PAG’ henceforth). Each of these components has a key role to play. PF127 is well-known to be a stabilizing surfactant for laponite particles: it adsorbs on the particle faces and provides steric stabilization.<sup>17</sup> Photoacid generators (PAGs) are commercially available organic molecules that have a key property: when irradiated with UV light, the molecules are photolysed, with one of their photoproducts being an acidic moiety.<sup>19,34-36</sup> As a result, the solution pH drops by an amount proportional to the PAG concentration (this can be as much as 3 pH units). While a variety of PAGs are available, the PAG chosen here has a relatively high solubility in water.<sup>19,37</sup>

Briefly, the mechanism behind the photogelling is as follows: initially, the particles are in a stable dispersion at pH 10 as they are covered by PF127 molecules. At this stage, both the particle edges and faces are negatively charged. Upon UV irradiation, the pH drops and this induces the charge on the particle edges to transform from negative to positive.<sup>15,33</sup> At the same time, the PF127 desorbs from the particle faces and forms micelles in solution. The positively charged particle edges then come in contact with the negatively charged particle faces and this leads to a connected network of particles (called a “house-of-cards” structure in the literature<sup>12,15,16,33</sup>). Support for the above mechanism is provided by a series of systematic experiments along with data from dynamic light scattering (DLS) and small-angle neutron scattering (SANS).

In closing this section, it is worth reiterating that the three components of the present PR fluids (i.e., laponite, PAG, and PF127) are all commercially available and relatively inexpensive. Thus, our results can be replicated easily by other researchers,

especially those who have an interest in putting PR fluids to use in microscale applications. Secondly, it is worth pointing out the analogy between our PR system with existing electrorheological (ER) fluids<sup>2</sup> and magnetorheological (MR) fluids<sup>38</sup>. ER and MR fluids are those whose rheology can be modulated by external electric or magnetic fields, respectively. Both types of fluids are dispersions of micron-sized particles in a solvent; in the “off” state, the particles are unconnected and the sample is of low viscosity, whereas when the field is switched on, the particles get connected into a network and the sample develops a yield stress.<sup>2,38</sup> The same mechanism underlies the behavior of our PR system as well. To our knowledge this is the first demonstration of a nanoparticle-based photorheological fluid.

### 3.2 Experimental Section

**Materials.** Laponite RD was obtained from Southern Clay Products. The nanoparticles are disklike with a diameter of 25 nm and a thickness of 0.92 nm. Pluronic F127 (PF127) was reagent grade and was purchased from Sigma Aldrich. The material is a triblock copolymer of the form PEO-PPO-PEO, where PEO refers to poly(ethylene oxide) and PPO to poly(propylene oxide). The percentages of PEO and PPO are ~ 70% and 30% respectively and the overall molecular weight is 12 kDa. The PAG, diphenyliodonium-2-carboxylate monohydrate, was purchased from TCI America (purity > 98%). Ultra-pure deionized water from a Millipore water-purification system was used in preparing samples for rheological characterization, while D2O (99.95% deuterated, from Cambridge Isotopes) was used for the SANS studies.

**Sample Preparation.** Dispersions of laponite particles were prepared by adding the particles to water, followed by vortex mixing for 5 min. A Branson 1510 sonicator was then used for 1 h at 40 kHz to fully disperse the particles. Weighted quantities of PF127 were then added to the laponite dispersions and the mixture was stirred for 1 h using a magnetic stirrer bar. Thereafter, weighted quantities of the PAG were added to the dispersion. Samples were stirred continuously overnight to fully dissolve the PAG and to ensure that the final sample was completely homogeneous.

**Sample Response Before and After UV Irradiation.** Laponite/PF127/PAG samples were irradiated with UV light from an Oriel 200 W mercury arc lamp. A dichroic beam turner with a mirror reflectance range of 280 to 400 nm was used to access the UV range of the emitted light. Samples (5-15 mL) were placed in a 20 mL vial with a quartz cover and irradiation was done for a specific duration under stirring. Alternately, 1 mL samples were placed in a 3 mL vial with a quartz cover and irradiation was done without stirring. Irradiated samples did not undergo any changes when stored under ambient conditions, which facilitated subsequent tests using techniques such as rheology and SANS.

**Rheological Studies.** Steady and dynamic rheological experiments were performed on an AR2000 stress controlled rheometer (TA Instruments, Newark, DE). Samples were run at 25°C on a cone-and-plate geometry (40-mm diameter, 4° cone angle) or a couette geometry (rotor of radius 14 mm and height 42 mm, and cup of radius 15 mm). To minimize loading effects on the gel samples, experiments were performed 1 h after



loading. Dynamic frequency spectra were obtained in the linear viscoelastic regime of each sample, as determined by dynamic stress-sweep experiments.

**Dynamic Light Scattering (DLS).** DLS measurements were made on a Photocor-FC light scattering instrument with a 5 mW laser light source at 633 nm with a scattering angle of 90°. A logarithmic correlator was used to measure the intensity autocorrelation function, from which the hydrodynamic radius was obtained by analysis using the method of cumulants coupled with the Stokes-Einstein equation.

**Small Angle Neutron Scattering (SANS).** SANS measurements were made on the NG-7 (30 m) beamline at NIST. Neutrons with a wavelength of 6 Å were selected. Three sample-detector distances of 1, 4 and 13 m were used to probe wave vectors from 0.004 to 0.4 Å<sup>-1</sup>. Samples were studied in 2 mm quartz cells at 25°C. Scattering spectra were corrected and placed on an absolute scale using calibration standards provided by NIST.

**SANS Modeling.** The SANS intensity  $I(q)$  from a structured fluid containing  $n_p$  particles per unit volume can be expressed in the following manner:

$$I(q) = n_p \cdot P(q) \cdot S(q) \quad (3.1)$$

where  $P(q)$  is the form factor and  $S(q)$  the structure factor.  $P(q)$  is the scattering that arises from *intra*-particle interference, which is a function of the particle size and shape.  $S(q)$  arises from *inter*-particle interactions and reflects the spatial arrangement of particles. When the particles are in dilute solution or are non-interacting, the structure factor  $S(q) \rightarrow 1$  and the intensity  $I(q)$  can be modeled purely in terms of the form factor  $P(q)$ . When

particles form networks,  $S(q)$  is no longer equal to 1 and we need to fit data considering both form and structure factors. In this study, we have used two form factor models (core-shell disks, spheres) and a structure factor model for fractal networks.

Form factor for core-shell spheres<sup>39</sup>:

$$P_2(q) = \frac{1}{\langle V_m \rangle} \int_0^{r=\infty} f(r) F^2(qr) dr \quad \text{where } F(qr) = p^3 (\rho_c - \rho_s) V_m \frac{3J_1(qpr)}{qpr} + (\rho_s - \rho_{solv}) V_m \frac{3J_1(qr)}{qr}$$

$$f(r) = (z+1)^{z+1} x^z \frac{\exp[-(z+1)x]}{r_{avg} \Gamma(z+1)} \quad \text{In which, } x = \frac{r}{r_{avg}}, z = \frac{1}{s^2} - 1, s = \frac{\sigma}{r_{avg}} \text{ is the polydispersity.}$$

**Parameters:**  
 $\langle V_m \rangle$  = average volume of sphere  
 $V_m$  = volume of the sphere  
 $r$  = overall radius (core+shell)  
 $pr$  = radius of core  
 $\rho_c$  = scattering length density of the core  
 $\rho_s$  = scattering length density of the shell  
 $\rho_{solv}$  = scattering length density of the solvent  
 $f(r)$  = Schulz distribution for the polydispersity of the radius

(3.2)

Form factor for core-shell disks<sup>17</sup>:

$$P_1(q) = \frac{1}{\langle V_p \rangle} \int_0^{R_p = \infty} n(R_p) F(q) dR_p$$

Where  $n(R_p) = \frac{\exp\left[-\frac{1}{2}\left(\frac{\ln R_{avg} - \ln R_p}{\sigma}\right)^2\right]}{(2\pi)^{1/2} \sigma R_p}$

$$F(q) = \frac{1}{\langle V_p \rangle} \int_0^{\pi/2} \sin\theta d\theta \left\{ V_1(\rho_1 - \rho_{solv}) \frac{\sin[q(H_p + 2\Delta H)(\cos\theta)/2]}{q(H_p + 2\Delta H)(\cos\theta)/2} \frac{2J_1[q(R_p + \Delta R)\sin\theta]}{q(R_p + \Delta R)\sin\theta} + V_p(\rho_p - \rho_1) \frac{\sin[qH_p(\cos\theta)/2]}{qH_p(\cos\theta)/2} \frac{2J_1[qR_p\sin\theta]}{qR_p\sin\theta} \right\}^2$$

in which  $J_1(x) = \frac{\sin x - x \cos x}{x^2}$  (3.3)

<p><b>Parameters (Core):</b>  <math>\langle V_p \rangle</math> = average volume of core  <math>V_p</math> = volume of core  <math>R_p</math> = radius of core = 25 nm  <math>H_p</math> = thickness of core = 0.9 nm  <math>\rho_p</math> = scattering length density of the core  <math>n(R_p)</math> = log-normal distribution for the polydispersity of particle radius</p>	<p><b>Parameters (Shell):</b>  <math>\Delta R</math> = shell thickness on the edge  <math>\Delta H</math> = shell thickness on the face  <math>\rho_1</math> = scattering length density of the shell</p>
<p><b>Parameters (Other):</b>  <math>V_1</math> = total volume of particle core and shell  <math>\rho_{solv}</math> = scattering length density of the solvent</p>	

Fractal structure factor<sup>40</sup>:

$$S_1(q) = 1 + \frac{D}{r_0^D} \int_0^\infty l^{D-1} \exp\left(-l/\xi\right) \frac{\sin(ql)}{ql} dl$$
 (3.4)

<p><b>Parameters:</b>  <math>D</math> = fractal dimension  <math>\xi</math> = correlation length</p>	<p><math>r_0</math> = effective radius of the particles  <math>l</math> = distance between particles</p>
--	--

### 3.3. Results and Discussion

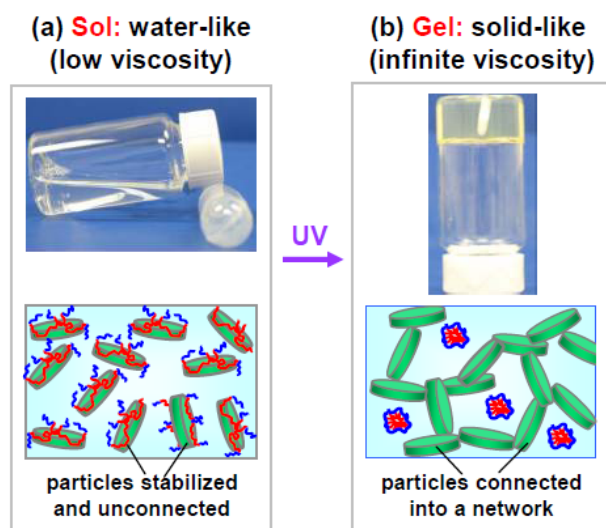


**Figure 3.2.** Photogelling of a 3% laponite + 3.6% PF127 + 13 mM PAG sample. Initially (a), the sample is a low-viscosity fluid: the particles are unconnected and stabilized by the adsorbed PF127. Upon UV irradiation (b), the particles assemble into a “card-house” network, causing the fluid to gel. In this case, the PF127 no longer covers the particle surface; instead it forms discrete micelles in solution. Note that the photogel holds its weight in the inverted vial and the stirrer bar is trapped in it.

**Photogelling: Rheological Studies.** Our photogelling samples are mixtures of laponite, PF127, and PAG in deionized water. Figure 3.2 shows photographs of a sample of 3% laponite together with 3.6% of PF127 and 13 mM of PAG. Initially, such dispersions are stable, low-viscosity sols. It is known that PF127 (Figure 3.1b) imparts steric stabilization to laponite dispersions: as indicated by the schematic in Figure 3.2a, the hydrophobic PPO segment of PF127 (shown in red) adsorbs onto the faces of the particles while the hydrophilic PEO segments (shown in blue) stretch out into the water.<sup>17</sup> The addition of the PAG has no effect on dispersion stability or the sample viscosity: samples remain unchanged for months. The above laponite/PF127/PAG sample is then subjected to UV light, whereupon the PAG is photolyzed to benzoic acid and iodobenzene (Figure

3.1c).<sup>19,35</sup> The macroscopic outcome of UV irradiation for 20 min is shown by the photograph in Figure 3.2b: the low-viscosity sol has been transformed into a strong gel that holds its weight in the inverted vial. Note that the stirrer bar remains trapped in the gel.

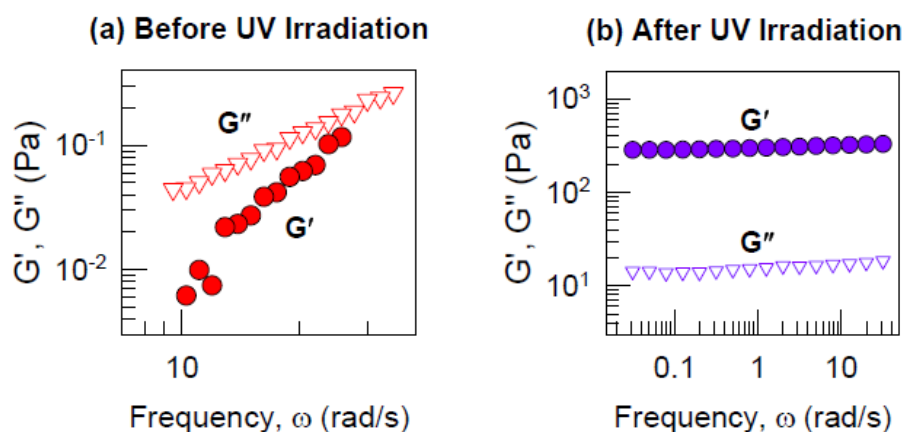


**Figure 3.3.** Dynamic rheology of a 1.4% laponite + 1.7% PF127 + 13 mM PAG sample (a) before and (b) after 15 minutes of UV irradiation. Before UV irradiation, the sample shows a purely viscous response, characteristic of a liquid. After irradiation, the sample response is purely elastic and characteristic of a gel. The gel modulus is about 300 Pa.

To quantify the light-induced changes in rheological properties, we first turned to dynamic rheology. Figure 3.3 shows typical dynamic rheological data (elastic modulus  $G'$  and viscous modulus  $G''$  as functions of frequency  $\omega$ ) for a sample before and after UV irradiation. The sample contains 1.4% laponite, 1.7% PF127 and 13 mM PAG. Before UV irradiation, the response of the sample is that of a purely viscous sol:  $G'' > G'$ , with both  $G'$  and  $G''$  being strong functions of frequency.<sup>20</sup> On the other hand, after 15 min of UV irradiation, the sample has been drastically altered: its response is now purely elastic,

as is characteristic of a permanent gel. That is,  $G' \gg G''$ , with both moduli being independent of frequency.<sup>20</sup> The gel modulus  $G_0$  is the value of the elastic modulus  $G'$  as the frequency  $\omega \rightarrow 0$  and is  $\sim 300$  Pa. Thus, a light-induced sol-gel transition is confirmed by the dynamic rheological data.

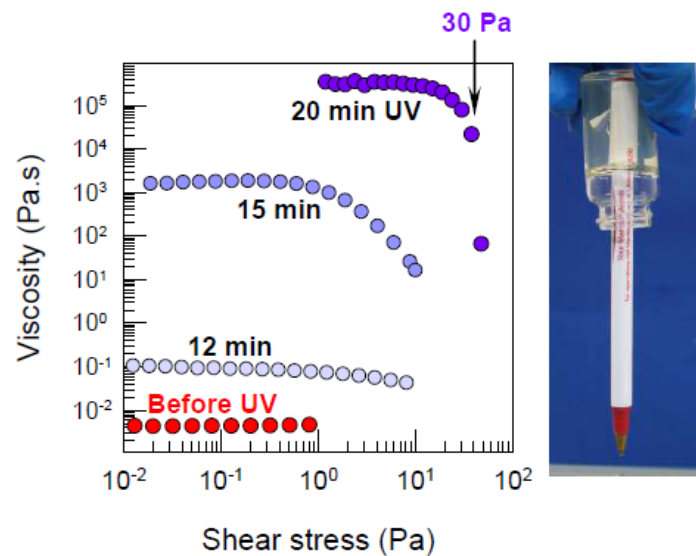


**Figure 3.4.** Steady-shear rheology of a 3% Laponite + 3.6% PF127 + 13 mM PAG sample before and after UV irradiation for various periods of time. The sample switches from a low-viscosity, Newtonian fluid to a strong gel with progressive irradiation. The final gel has a yield stress of  $\sim 30$  Pa, which is sufficient to hold the weight of a pen.

Figure 3.4 shows steady-shear rheological data (viscosity vs. shear stress) on a photogelling sample. The data also simultaneously illustrates the time-dependence of the light-induced changes. The sample is 3% laponite + 3.6% PF127 + 13 mM PAG (same as in Figure 3.2). Before UV irradiation, the sample is a Newtonian liquid with a low viscosity of 4.4 mPa.s (i.e., about 4 times the viscosity of the solvent, water). After 12 min of irradiation, the zero-shear viscosity  $\eta_0$  (i.e., the viscosity at low shear-stresses or

shear-rates) is increased by a factor of  $\sim 20$  and the sample shows weak shear-thinning. By the 15 min mark,  $\eta_0$  has been further increased by another four orders of magnitude and the sample becomes strongly shear-thinning. After 20 min,  $\eta_0$  is essentially infinite at low stresses (i.e., the sample is a gel). The sample has a finite yield stress of about 30 Pa: this is the value of the stress at which the viscosity begins to plummet (see arrow, note this is an approximate value). Note that this yield stress is high enough to support the weight of an embedded pen, as shown by the photograph in Figure 3.4. We should point out here that the rate of photogelling is limited by the rate of absorption of UV light by the sample (PAG photolysis itself occurs in nanoseconds<sup>36</sup>). Thus, photogelling can be hastened by using higher intensity lamps and/or smaller sample volumes (path lengths).<sup>10,11</sup>

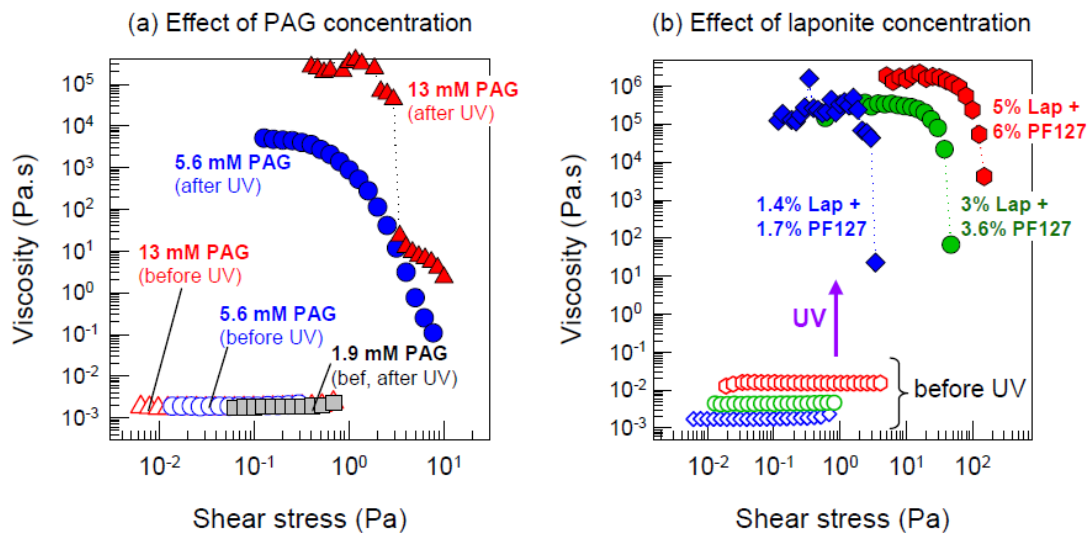


**Figure 3.5.** (a) Effect of PAG concentration on photogelling. Steady-shear data are shown for samples containing 1.4% laponite + 1.7% PF127 + various amounts of PAG before and after 15 min of UV irradiation. (b) Effect of laponite concentration on photogelling. Steady-shear data before and after UV irradiation for 20 min are shown for samples containing 13 mM PAG with various amount of laponite + PF127. In both cases, data before UV are shown using unfilled symbols and after UV with filled symbols.

We now describe how the extent of photogelling varies with sample composition. First, Figure 3.5a shows the effect of PAG concentration. As stated earlier, addition of PAG has no influence on the initial viscosity of laponite+PF127 dispersions; thus, the initial viscosities for 1.9, 5.6, and 13 mM PAG overlap (the initial pH in all cases is about 9.6–9.8). However, the amount of PAG does influence the photogelling. If the PAG concentration is very low (1.9 mM), no light-induced viscosity increase is seen and the data before and after irradiation are identical. For moderate amounts of PAG (5.6 mM), the viscosity increases appreciably upon exposure to light. Finally, with sufficiently high PAG amounts (13 mM), the full extent of photogelling occurs. Further addition of PAG beyond 13 mM did not increase the yield stress of the photogel. Note that the higher the PAG concentration, the lower the pH after irradiation: the pH values were 8.5, 7.8 and 7.4, respectively, for 1.9, 5.6, and 13 mM PAG. The light-induced reduction in pH is one key aspect in the mechanism for photogelling, as will be discussed later.

The strength of the photogel can also be modulated by varying the concentration of laponite particles. Figure 3.5b shows rheology data before and after UV irradiation for 3 samples, all containing 13 mM of PAG. The laponite concentration is varied from 1.4% to 3% to 5% and the PF127 concentration is proportionately increased to keep the particles stable initially. With increasing laponite, the initial viscosity of the sample is marginally higher, while the sample response remains Newtonian in all cases. All three samples are gelled by exposure to UV, with the yield stress of the photogel increasing



from 3 Pa for the 1.4% sample to 30 Pa for the 3% sample and finally to 100 Pa for the 5% laponite sample.

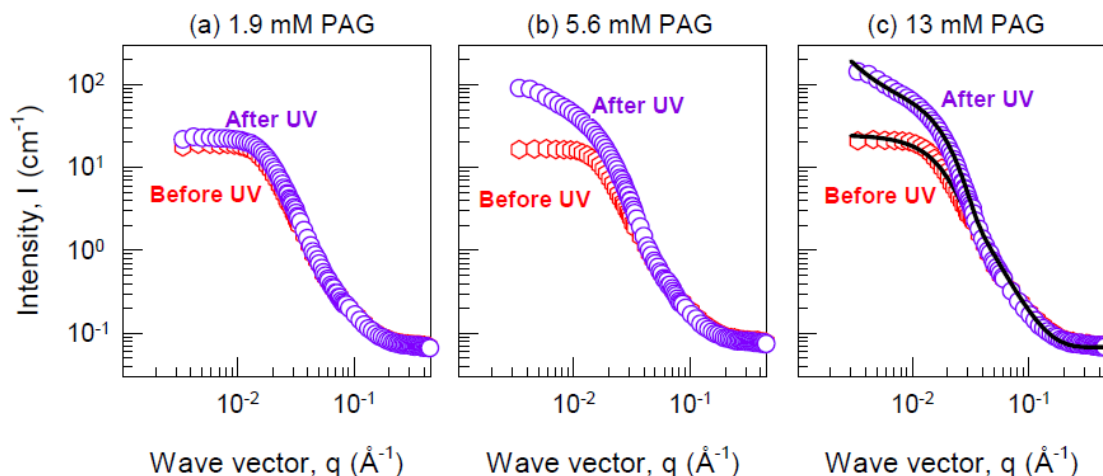


**Figure 3.6.** SANS scattering spectra (intensity  $I$  vs. wave-vector  $q$ ) for samples containing 1.4% laponite + 1.7% PF127 and with three different PAG concentrations. Data before UV irradiation are shown as red symbols and that after 15 min of UV irradiation are shown as violet symbols. For the 13 mM PAG sample, the data before and after UV are fit to models as described in the text, and the model fits are shown as solid lines.

**Photogelling: SANS Studies.** The results so far provide clear experimental evidence for photogelling in laponite/PF127/PAG samples. We can attribute this effect to a transition from unconnected laponite particles before irradiation to a 3-D network of the same particles after irradiation, as shown by Figure 3.2. To substantiate this mechanism, we first resorted to SANS. Samples were made in  $D_2O$  to attain the required contrast between the structures of interest and the solvent: these samples were visually and rheologically identical to those in  $H_2O$ . Figure 3.6 shows SANS spectra ( $I$  vs.  $q$ ) for 1.4% Laponite+1.7% PF127 dispersions at three different PAG concentrations: 1.9, 5.6 and 13 mM. Data are provided both before and after UV irradiation. Before irradiation, the data

are identical at the three PAG concentrations, which is consistent with the rheological data in Figure 3.5a. In all cases, the scattering intensity shows a plateau at low- $q$ , which suggests that there is no large-scale particle aggregation, i.e., the laponite particles are initially well-dispersed. After irradiation, a significant rise in low- $q$  scattering intensity is seen for the samples that photogel (5.6 and 13 mM PAG). In comparison, there is no increase in low- $q$  scattering intensity for the 1.9 mM PAG sample that does not photogel as per Figure 3.5a. A rise in low- $q$  intensity signifies growth of large structures and/or attractive interparticle interactions.<sup>23</sup> Thus, we can directly infer a change from unconnected to connected particles even without the benefit of insights from modeling.

**Table 3.1.** Key parameters of SANS modeling for 1.4% laponite + 1.7% PF127 + 13 mM PAG before and after 15 min UV irradiation.

Parameters	Before UV	After UV
Edge shell thickness (nm)	$0.5 \pm 0.016$	$0 \pm 0.015$
Face shell thickness (nm)	$1.5 \pm 0.002$	$0.3 \pm 0.009$
Micelle core diameter (nm)	$1.6 \pm 0.013$	$12 \pm 0.056$
Micelle shell thickness (nm)	$0.4 \pm 0.008$	$2 \pm 0.015$
Fractal dimension	None	$2 \pm 0.02$

We have also fit models to the SANS data in Figure 3.6c. Details of the models used are provided in the Experimental Section (eq 3.1-3.4). Important model parameters are listed in table 3.1. For the initial system of stabilized particles, we model the laponite covered by PF127 as core-shell disks, as has been done by Nelson and Cosgrove.<sup>17</sup> The laponite core is fixed to have a diameter of 25 nm and a thickness of 0.9 nm while the dimensions of the PF127 shell are obtained from model fitting: shell thicknesses of 1.5 nm over the particle face and 0.5 nm over the particle edge are obtained. All these dimensions are consistent with previous reports.<sup>17,41</sup> In addition to the stabilized particles,

the presence of discrete micelles of PF127 in the solution must also be included in the model.<sup>17</sup> Again, consistent with the literature, these molecules are considered to be core-shell spheres with a PPO core and a PEO shell.<sup>42</sup> From the model fit,<sup>39</sup> a core diameter of 1.6 nm and a shell thickness of 0.4 nm are estimated for these micelles. Note that no structure factor needs to be included to model the system before UV; our model only takes into account the form factors of the PF127-covered laponite particles and of the free PF127 micelles. The fact that a structure factor is not needed confirms our assumption that the particles are discrete and experience no significant long-range interactions.<sup>23</sup>

Next, we consider the same system after UV irradiation, i.e., after it has undergone photogelling. In this case, the particles are expected to be connected into a volume-filling network. We therefore include a fractal structure factor<sup>39,40</sup> in the model for the laponite particles, in addition to the form factors from above (i.e., core-shell disks for the particles, core-shell spheres for the PF127 molecules/micelles). From the model fit, we obtain a fractal dimension of 2 for the laponite gel, consistent with the findings of Pignon *et al.*<sup>43</sup> With regard to the particles, the shell dimensions are reduced to near zero, indicating that the particles are mostly just the laponite core; i.e., the PF127 is no longer adsorbed on the particles. The desorbed PF127 forms micelles in solution having a core diameter of 12 nm and a shell thickness of 2 nm. The larger dimensions for the micelles following UV indicate that they are composed of numerous PF127 chains; also, they likely encapsulate the hydrophobic byproduct of the photolysis (iodobenzene) in their core. All in all, SANS modeling provides numerous insights which are used below in formulating a detailed photogelling mechanism.

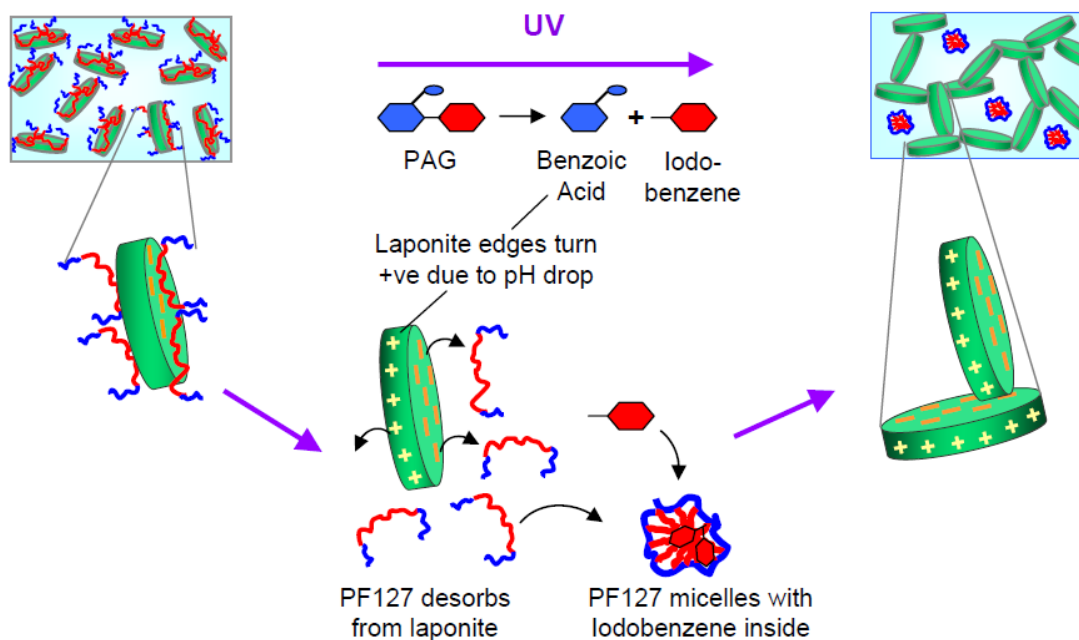


**Figure 3.7.** Mechanism for photogelling. Initially, laponite disks are stabilized by PF127, with the hydrophobic PPO portion (red segment) of PF127 adsorbed on the particles and the hydrophilic PEO portions (blue) extending into water. Upon UV irradiation, the PAG splits into benzoic acid and iodobenzene. The PF127 desorbs from the laponite and forms micelles in solution, taking up the hydrophobic iodobenzene. The lowering of pH by the benzoic acid causes the particle edges to turn positive. In turn, the particles assemble into a network due to interactions between the positive edges and the negative faces.

**Photogelling: Mechanism.** We now put forth a mechanism for photogelling, illustrated in Figure 3.7, starting from molecular events and correlating these to structural transitions. Initially (before irradiation), we have a sol of laponite/PF127/PAG, with the particles stabilized and unconnected. Upon UV irradiation, we end up with a gel, with the laponite particles connected into a network. How does UV light transform the sol into a gel? The only light-sensitive component of the system is the PAG, and PAG photolysis gives rise to benzoic acid and iodobenzene (Figure 3.1c).<sup>19,35</sup> An obvious question then is

whether addition of benzoic acid and iodobenzene to a laponite/PF127 sol can convert it into a gel. We have tested this, and the results are schematically captured in Figure 3.8a. As an example, consider a stable sol of 1.4% laponite and 1.7% PF127. If benzoic acid *alone* or iodobenzene *alone* are added to this sample, no gelling occurs regardless of the concentration of the additives. On the other hand, if 13 mM of benzoic acid and iodobenzene *are both added*, gelling does occur – this indicates that each component of PAG photolysis has a crucial role to play.

A key related insight into laponite particles is that, as pH drops below 9, laponite particle edges acquire a positive charge,<sup>15,33</sup> which allows their interactions with negatively charged faces and leads to a network of particles. Such a network is called a “house-of-cards” gel.<sup>12,15,16,33</sup> In our system, we believe the photolysis products of the PAG work in tandem to drive a transition from a sol to a house-of-cards gel. In particular, *the iodobenzene drives the PF127 molecules off the laponite particles, while the benzoic acid lowers the solution pH from ~ 10 to ~ 8 and thereby make the laponite edges positively charged.* Both these events are depicted in Figure 3.7. Note that iodobenzene is hydrophobic, and while a few molecules may adsorb on the laponite, most will get solubilized in PF127 micelles (also depicted in Figure 3.7). In either case, PF127 that was previously adsorbed will be driven into solution in the form of micelles. The absence of the steric barrier provided by PF127 will allow the negatively charged laponite faces to interact with the positively charged laponite edges and form a house-of-cards gel,<sup>12,15,16,33</sup> as shown in the right-hand panel of Figure 3.7.

Many disparate pieces of evidence have been used to put together the above mechanism. Some have been mentioned earlier: e.g., the drop in sample pH upon UV irradiation was discussed in the context of Figure 3.5a; also, the parameters from SANS modeling are consistent with the desorption of PF127 from the laponite particles upon UV irradiation. Further support is provided a study on iodobenzene addition to a solution of PF127. While iodobenzene is not soluble in pure water, it does get solubilized in the presence of PF127. In fact, we have found that *iodobenzene induces PF127 micelles*: e.g., a 1.7% PF127 solution gave no indication of micelles by DLS whereas upon addition of 13 mM iodobenzene, micelles with a diameter of 28 nm were measured in the solution by DLS. This result implies that it is possible for the PF127 adsorbed on laponite to desorb and form micelles when iodobenzene is added. Again, note that desorption of PF127 from the particles is not sufficient for gelling: the pH must also be reduced to alter the charge on the particle edges. Such a pH reduction can be induced by benzoic acid, which explains the results of Figure 3.8a. Note that benzoic acid is not unique in this context: any other acid like HCl can also be used to lower the pH and thereby cause gelation.

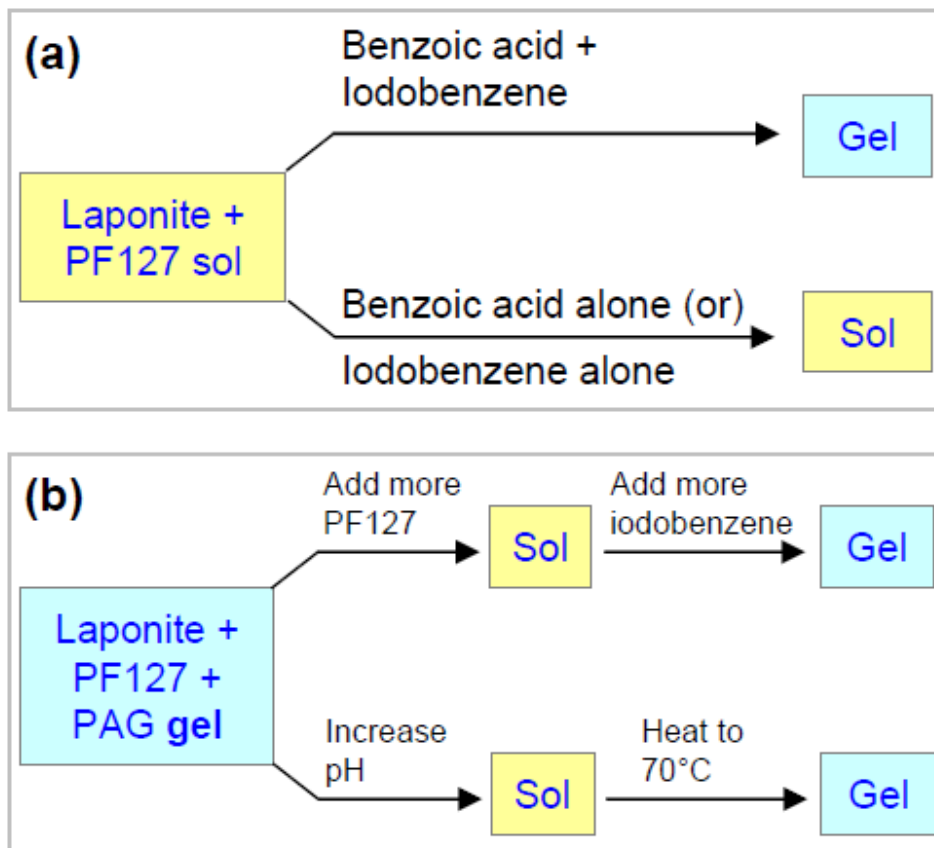


**Figure 3.8.** Schematics of experiments that give insight into the photogelling mechanism. (a) A sol of laponite+PF127 can be gelled if both iodobenzene and benzoic acid are added, but not if only one of the two are added. (b) A gel of laponite+PF127+PAG can be liquefied (ungelled) by either adding more PF127 or by increasing the pH. The former can be gelled again by adding more iodobenzene. The sols are also temperature sensitive and can be gelled by heating to 70° C.

Finally, we should mention that a photogelled laponite/PF127/PAG sample can be ungelled (converted back to a low-viscosity fluid) in a couple of different ways (Figure 3.8b), both of which are consistent with the above mechanism. First, adding more PF127 to a photogel will ungel it, and if iodobenzene is subsequently added, the solution can be gelled again. This result means that if PF127 is replenished on the particle surface, there will be no gel; if the new PF127 is driven off the particles by fresh iodobenzene, the gel will form again. Second, the photogel can be ungelled by increasing the pH back to ~ 10,

e.g., by adding NaOH or other bases. This result confirms the key role of pH in ensuring positively charged particle edges, which are needed for gelation.<sup>15,33</sup> Intriguingly, this means that our system is not only responsive to light but also to a different stimulus, pH. In fact, the same system is also responsive to temperature: the sol generated by an increase in pH can also be gelled by heating the sample to  $> 70^{\circ}\text{C}$  (Figure 3.8b). The temperature-response is not fully understood and is being investigated in more detail. Nevertheless, it is striking that a single complex fluid can show sensitivity to a variety of commonly studied stimuli: light, pH and temperature.

### **3.4. Conclusions**

We have demonstrated UV-induced photogelling in laponite/PF127/PAG mixtures. Initially, the PF127 is adsorbed on the faces of laponite particles, which sterically stabilizes them from aggregation. Upon UV irradiation, the PAG is photolyzed into benzoic acid and iodobenzene. The formation of benzoic acid drops the solution pH from 10 to 8, which in turn makes the particle edges positively charged. The iodobenzene, on the other hand, drives the PF127 off the particle faces and into solution where the PF127 forms micelles with iodobenzene in its cores. This frees up the particle edges (+) and faces (-) for interaction, which drives the assembly of a house-of-cards network. The water-like sol is thus transformed into a stiff elastic gel having a sufficient yield stress to hold its own weight or the weight of small embedded objects.



## Chapter 4

# Reversible Thermogelling of Nanoparticle Dispersions

---

### 4.1. Introduction

Temperature is a variable that can profoundly affect the rheology of complex fluids. The majority of structured complex fluids, including polymer solutions and gels<sup>44-48</sup>, wormlike micellar solutions<sup>49-52</sup>, supramolecular gels<sup>53</sup>, and nanoparticle dispersions<sup>54</sup> etc. show a decrease in their rheological properties upon heating. The decrease could occur progressively and steadily with increasing temperature, as is the case for many polymer solutions, or it could be abrupt (akin to melting), as is the case for an aqueous gel of gelatin (Jello®), for example. In comparison, the opposite behavior, i.e., an increase in rheological properties with heating, is observed in only a few systems, including some based on polymers,<sup>55-57</sup> surfactants,<sup>58,59</sup> or other hybrid supramolecules<sup>60</sup>. In some of these cases, the fluid viscosity shows a finite increase over a range of temperatures, and this behavior is termed thermo-thickening. Alternately, the system can show a true liquid-to-solid (sol-gel) transition upon heating and such behavior is referred to as *thermogelling*.

Thermogelling fluids can have applications in areas such as heat-baked paints and coatings<sup>61</sup>, drug delivery and cancer therapy<sup>55,62</sup>, microfluidics<sup>63</sup> and capillary electrophoresis<sup>64-67</sup>, and in fire-fighting<sup>68</sup>. In the case of biomedical applications such as

drug delivery, the utility of thermogelling fluids is if they can be injected as thin solutions at room temperature but would rapidly form gels at body temperature<sup>62</sup> – the gelation would then serve to localize an embedded drug. In fire-fighting, a product termed Thermo-Gel® has been commercialized<sup>68</sup> – basically water containing a thermogelling agent – has proven to be more effective at putting out fires because of its ability to undergo gelling with heat. Apart from applications, thermogelling is also an intriguing phenomenon because it is so counter-intuitive and rare – and therefore worthy of study.

During the course of our studies in Chapter 3, we found that mixtures of laponite and the triblock copolymer, Pluronic F127 (PF127) can show thermogelling. This Chapter describes a detailed investigation into this phenomenon. To recap the details of the system, laponite is a synthetic clay that exists as nanoscale disks, 25 nm in diameter and 0.9 nm in thickness. PF127 is well-known to provide steric stabilization to laponite particles. Interestingly, PF127 on its own in water exhibits thermogelling, but only in concentrated solutions ( $> 15$  wt%)<sup>69</sup>. This is known to involve a transition from small discrete micelles of PF127 at low temperatures to an ordered cubic phase of larger micelles at high temperatures<sup>69</sup>. In the systems studied here, the PF127 is present at much lower concentrations ( $\sim 1-6$  wt%) and does not undergo thermogelling on its own. Dispersions of laponite in water with no additives also do not show thermogelling. However, aqueous mixtures of a few wt% each of laponite and PF127 undergo a sharp gelation upon heating. The phenomenon is robust, occurring also in the presence of inert additives, such as pigment particles. It is reversible, i.e., the sample reverts to a sol upon

cooling. The likely mechanism for thermogelling involves depletion flocculation of laponite particles induced by PF127 micelles.

## 4.2. Experimental Section

**Materials.** Laponite RD was obtained from Southern Clay Products. The nanoparticles are disklike with a diameter of 25 nm and a thickness of 0.92 nm. Pluronic F127 (PF127) was reagent grade and was purchased from Sigma Aldrich. The material is a triblock copolymer of the form PEO-PPO-PEO, where PEO refers to poly(ethylene oxide) and PPO to poly(propylene oxide). The percentages of PEO and PPO are ~ 70% and 30% respectively and the overall molecular weight is 12 kDa, leading to an approximate formula of  $(EO)_{106}(PO)_{70}(EO)_{106}$ . Ultra-pure deionized water from a Millipore water-purification system was used in preparing samples for rheological characterization, while  $D_2O$  (99.95% deuterated, from Cambridge Isotopes) was used for the SANS studies. The titania ( $TiO_2$ ) pigment particles were a gift from Sherwin Williams Co.

**Sample Preparation.** Dispersions of laponite particles were prepared by adding the particles to deionized water, followed by vortex mixing for 5 min. A Branson 1510 sonicator was then used for 1 h at 40 kHz to fully disperse the particles. Weighed quantities of PF127 were then added to the laponite dispersions and the mixture was stirred continuously overnight to ensure that the final sample was completely homogeneous. The pH value is ~10. For samples containing  $TiO_2$ , the latter particles were added to the laponite-PF127 dispersion and vortexed to get a homogeneous sample.

**Rheological Studies.** Steady and dynamic rheological experiments were performed on an AR2000 stress controlled rheometer (TA Instruments, Newark, DE). Samples were run on a cone-and-plate geometry (40 mm diameter, 4° cone angle) or a Couette geometry (rotor of radius 14 mm and height 42 mm, cup of radius 15 mm). For experiments at different temperatures, experiments were performed 20 min after equilibrating the loaded sample to the desired temperature. Dynamic frequency spectra were obtained in the linear viscoelastic regime of each sample, as determined by dynamic strain-sweep experiments.

**Small Angle Neutron Scattering (SANS).** SANS measurements were made on the NG-7 (30 m) beamline at NIST in Gaithersburg, MD. Neutrons with a wavelength of 6 Å were selected. Three sample-detector distances of 1, 4 and 13 m were used to probe wave vectors from 0.004 to 0.4 Å<sup>-1</sup>. Samples were studied in 2 mm quartz cells at 25°C and 80°C. Scattering spectra were corrected and placed on an absolute scale using calibration standards provided by NIST.

**Transmission Electron Microscopy (TEM).** TEM was conducted on a Jeol JEM 2100 microscope at 80 KeV. The staining agent, uranyl acetate (UA) (from Sigma-Aldrich), was dissolved in water to form a 1% stock solution. 1 µL of the laponite/PF127 sample was applied on a carbon/formvar coated copper grid, which was then dried at room temperature and 80°C. The dried TEM grid was then stained with a drop of the 1% UA solution and air-dried before imaging.

### 4.3. Results and Discussion

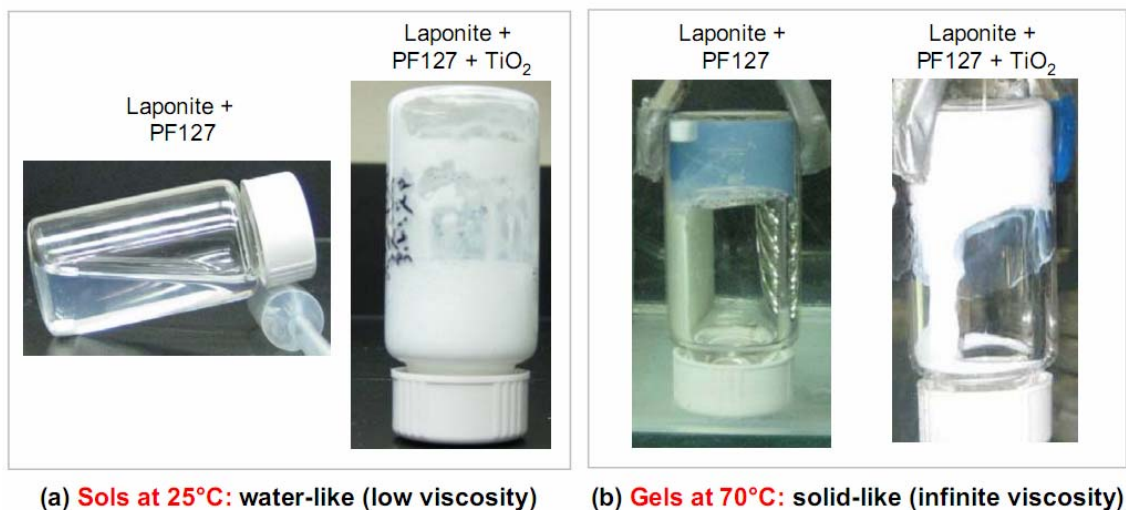


**Figure 4.1.** Thermogelling of a 3% laponite + 3.6% PF127 sample, both in its neat form as well as in conjunction with 40% of TiO<sub>2</sub> pigment particles. At room temperature or 25°C (a), the samples are low-viscosity, freely flowing fluids. At 70°C (b), both samples are transformed into gels. Note that the thermogels hold their weight in the inverted vials, indicating substantial yield stresses.

**Thermogelling: Rheological Studies.** First we describe visual observations of thermogelling. Our samples are mixtures of laponite and PF127 in deionized water. Figure 4.1a shows a photograph of a sample of 3% laponite and 3.6% PF127. At room temperature, the dispersion is a low-viscosity sol that flows freely in the vial. It is known that PF127 imparts steric stabilization to laponite particles, ensuring that the particles do not flocculate or aggregate<sup>17</sup>. Such sols remain unchanged even months after preparation. Next, in Figure 4.1b, the same sample is photographed while being held in a water bath at 70°C. The sample has been transformed into a gel at this higher temperature, as shown by its ability to hold its weight in the inverted vial. Note that the sample has a bluish hue but

is homogeneous. The stirrer bar can be clearly seen to be trapped in the gel. No evidence of liquid crystalline behavior (e.g., optical birefringence) was observed in the gel state.

The above thermogelling is robust and reproducible. The phenomenon is observed over a range of laponite and PF127 concentrations (see below). The addition of inert particles or polymers does not alter the behavior. For example, we considered titania ( $\text{TiO}_2$ ) pigment particles, which are routinely used in a variety of paints and coatings, including heat-baked coatings that are applied at high temperatures<sup>61</sup>. Could a coating be formulated with laponite and PF127 to control its high-temperature rheology? Figure 4.1 shows the same laponite/PF127 sample with 40% (w/w) of  $\text{TiO}_2$ . At low temperatures, the mixture is a homogeneous, stable, and freely flowing dispersion – note the white color of the sample due to the high concentration of the pigment. At 70°C, the same sample has been transformed into a gel, much like its pigment-free counterpart. This behavior suggests that laponite/PF127 mixtures can indeed be used as high-temperature rheology-modifying agents – at the same time, they will have little effect on the rheology at room-temperature.

We conducted rheological studies to quantify the temperature-induced changes in the above sample. Figure 4.2a shows its dynamic rheology (elastic modulus  $G'$  and viscous modulus  $G''$  as functions of frequency  $\omega$ ) at 25 and 70°C. At 25°C, the response is liquid-like:  $G'' > G'$ , with both  $G'$  and  $G''$  being strong functions of frequency.<sup>20</sup> On the other hand, the response at 70°C is solid-like:  $G' \gg G''$ , with both moduli independent of frequency.<sup>20</sup> The latter response is typical of a permanent gel. The frequency-independent

value of  $G'$  can be termed the gel modulus  $G_0$  and it is  $\sim 200$  Pa. Thus, dynamic rheology confirms the thermogelling transition in this sample.

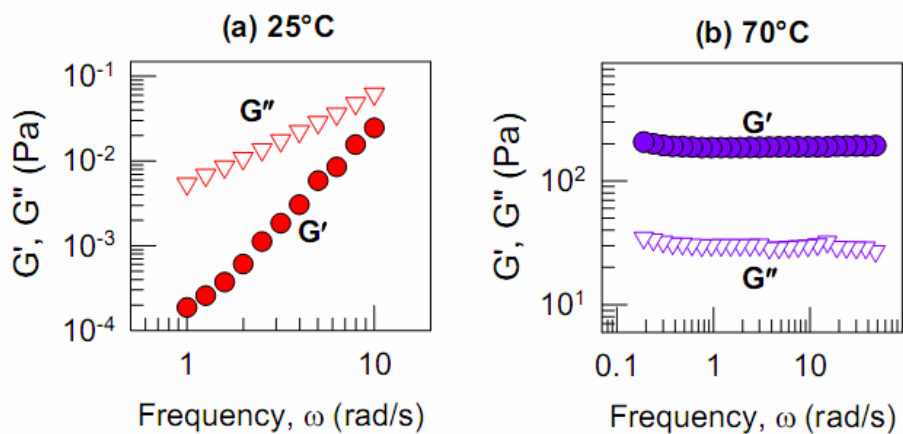


**Figure 4.2.** Dynamic rheology of a 3% laponite + 3.6% PF127 sample at (a) 25°C and (b) 70°C. At 25°C, the sample shows a viscous response, characteristic of a liquid. At 70°C, the sample response is elastic and characteristic of a gel.

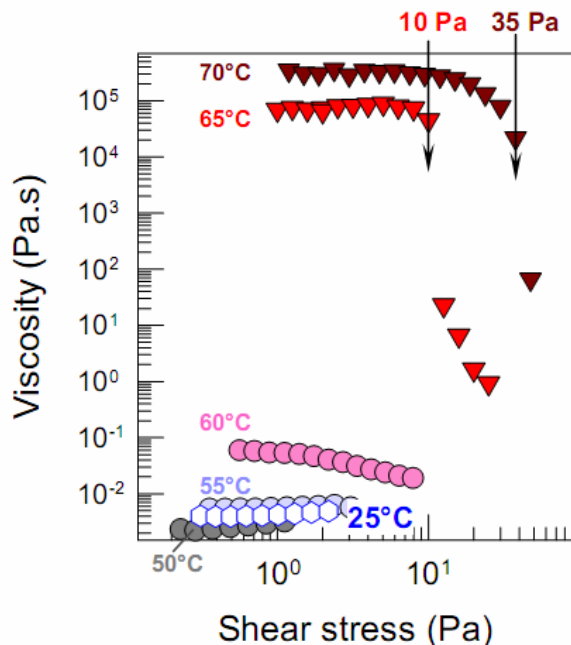
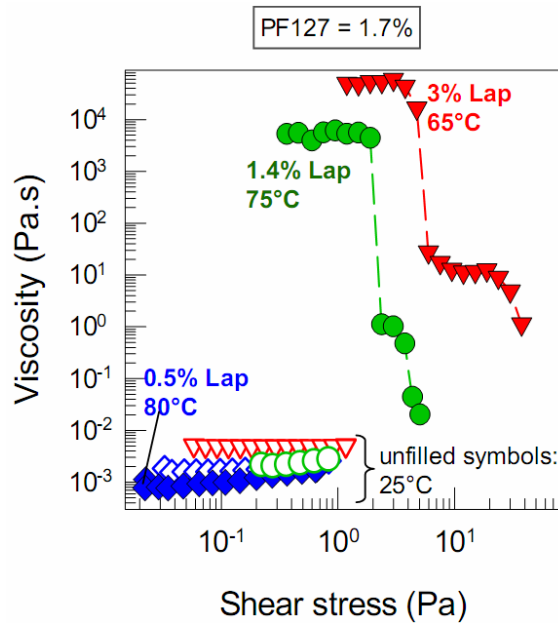


**Figure 4.3.** Steady-shear rheology of a 3% Laponite + 3.6% PF127 sample at different temperatures. Around 65°C, the sample abruptly transforms from a low-viscosity, Newtonian fluid to a gel-like sample having a yield stress (marked by arrows).

Figure 4.3 shows steady-shear rheological data (viscosity vs. shear stress) on the above sample over a range of temperatures between 25 and 70°C. At 25 °C, the sample is a Newtonian liquid with a viscosity of 4 mPa.s (i.e., about 4 times the viscosity of the solvent, water). At 50°C and 55°C, the sample remains Newtonian and with about the same viscosity. Around the 60°C mark, the viscosity begins to show a modest increase (by a factor of ~ 20). Further heating to 65°C causes a sharp change in the rheology as the sample transforms from a liquid to a gel or yield-stress fluid (Bingham plastic). The viscosity is found to be essentially infinite at low stresses below the yield stress, which is 10 Pa at this temperature (arrow). Above the yield stress, the viscosity plummets by several orders of magnitude. A further increase in temperature to 70°C causes an increase in the yield stress to about 35 Pa. Together, the data show that thermogelling is a sharp change in the sample at a distinct temperature.

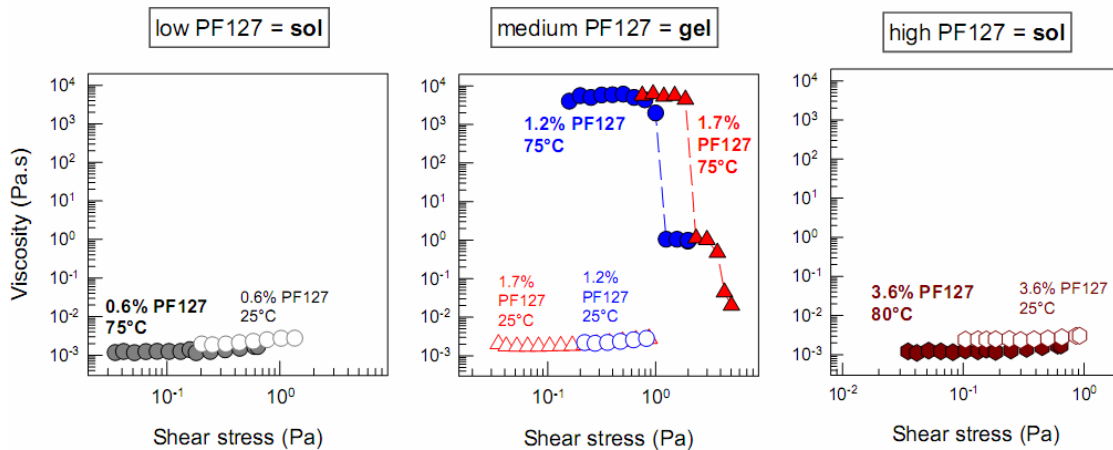
The sharp thermogelling transition in laponite/PF127 mixtures is distinctly reminiscent of the thermogelling in neat PF127<sup>63</sup> – however, as mentioned in the Introduction, the latter occurs only at much higher PF127 concentrations than those used here. The thermogelling of neat PF127 reflects the formation of a cubic phase of close-packed spherical micelles<sup>69,70</sup>. We will show that the phenomenon seen here is of a very different nature. In particular, thermogelling in laponite/PF127 mixtures requires that *both the components* be present at appropriate concentrations. This fact is brought out by the results in Figures 4.4 and 4.5, which are rheological plots for different compositions of the above mixtures at low and high temperatures.





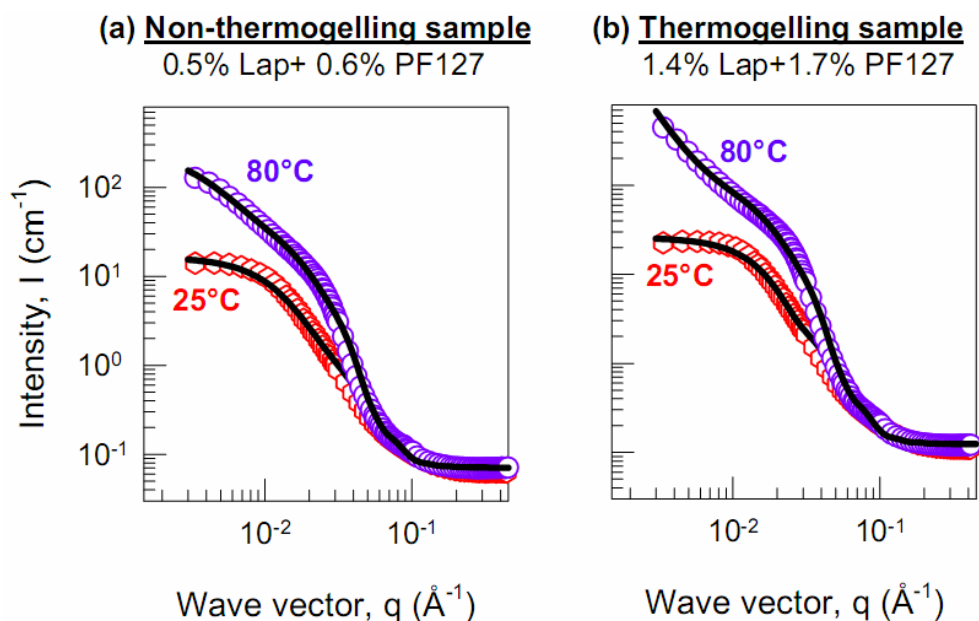
**Figure 4.4.** Effect of laponite concentration on thermogelling. Steady-shear data at 25°C and high temperatures are shown for samples containing 1.7% PF127 and varying amounts of laponite. Data at 25°C are shown using unfilled symbols and those at high temperatures are shown with filled symbols. Thermogelling occurs only for laponite concentrations above a minimum value.

Figure 4.4 shows the effect of laponite concentration on the thermogelling, which is studied at a constant PF127 content of 1.7%. All samples are thin, Newtonian liquids at low temperatures. If the laponite concentration is too low, e.g., 0.5%, no temperature-induced viscosity increase is seen – in fact, the viscosity at 80°C is slightly lower than that at 25°C. At a higher laponite amount of 1.4%, the system gels at 75°C with a yield stress of 2 Pa. Further increase Laponite to 3% reduces the gelling temperature to 65°C while the yield stress increases to 4 Pa. Thus, a minimum amount of laponite needs to be present for thermogelling. The lack of thermogelling at zero laponite or low amounts of laponite is clear evidence that the phenomenon is not simply due to the PF127.



**Figure 4.5.** Effect of PF127 concentration on thermogelling. Steady-shear data are shown for samples containing 1.4% laponite and varying amounts of PF127 at 25°C and high temperatures. Thermogelling occurs only at intermediate PF127 concentrations (panel B); it does not occur either at lower or higher concentrations of PF127.

The effect of PF127 concentration at constant laponite (1.4%) is even more interesting, as shown by the three panels in Figure 4.5. No thermogelling is seen for low amounts of PF127, e.g., 0.6% – the viscosity of this sample is again slightly lower at 80°C than at room temperature (Figure 4.5a). When the PF127 is increased to 1.2% or 1.7%, thermogelling does occur (Figure 4.5b). Both samples gel at 75°C, with the yield stress being slightly higher for the 1.7% sample. Thus, PF127 also needs to be present at a minimum level for thermogelling to occur. However, the more intriguing result is that shown by Figure 4.5c for an even higher PF127 content of 3.6%. In this case, the sample *does not* gel upon heating. We have reproduced this result many times, and the same holds true for even higher PF127 amounts (e.g., 5% or 7%). Taking the results in order at a temperature of ~ 75°C, we see that adding PF127 to laponite initially gives a sol, then a gel, and finally a sol again as the PF127 content is increased. Any postulated mechanism for thermogelling has to explain this unusual result.



**Figure 4.6.** SANS scattering spectra (intensity  $I$  vs. wave-vector  $q$ ) at 25 and 80°C for samples containing (a) 0.5% laponite + 0.6% PF127 and (b) 1.4% laponite +1.7% PF127. The data are fit to models (see text), and the model fits are shown as solid lines.

**Thermo-gelling: SANS Studies.** To gain insight into the thermogelling mechanism, we turned to SANS. Samples were made in  $\text{D}_2\text{O}$  to attain the required contrast between the structures of interest and the solvent: these samples were identical to those in water. Figure 4.6 shows SANS spectra ( $I$  vs.  $q$ ) for two samples at 25°C and 80°C. The first contains 0.5% laponite and 0.6% PF127 – this sample does not show thermogelling because the laponite and PF127 concentrations are low. The second sample, which contains 1.4% laponite and 1.7% PF127, does exhibit thermogelling at 75°C. Both samples exhibit similar features. At 25°C, the intensity  $I$  shows a plateau at low  $q$ , which suggests that the laponite particles are well-dispersed and stable. At 80°C, a significant rise in  $I$  at low  $q$  is seen for both samples. The only difference is that  $I$  seems to be tapering out for the non-thermogelling sample, whereas the  $I$  for the thermogelling one

continues to increase (diverges). Generally, an increase in  $I$  at low  $q$  signifies growth of large structures and/or attractive interactions between the particles.<sup>23</sup>

**Table 4.1.** Key parameters of SANS modeling for 0.5% laponite + 0.6% PF127 and 1.4% laponite + 1.7% PF127 at 25°C and 80°C.

Parameters	0.5% lap + 0.6% PF127		1.4% lap + 1.7% PF127	
	25°C	80°C	25°C	80°C
Edge shell thickness (nm)	1.6 ±0.013	2.8 ±0.027	1.6 ±0.007	2.8 ±0.019
Face shell thickness (nm)	1.6 ±0.001	5.4 ±0.006	1.6 ±0.001	5.4 ±0.004
Micelle core diameter (nm)	1.6 ±0.005	7.6 ±0.004	1.6 ±0.003	7.6 ±0.004
Micelle shell thickness (nm)	0.4 ±0.003	2.2 ±0.003	0.4 ±0.002	2.2 ±0.002
Cluster size (nm)	None	22.4 ±0.066	None	907 ±59.8

To model the SANS data, we make the following assumptions. The structures present in the samples will be: (a) laponite disks covered with adsorbed PF127; and (b) spherical PF127 micelles in the bulk. Initially, the disks will be distinct and unaggregated. Thus, the system can be modeled based on the form factors for core-shell disks (eq 3.2) and core-shell micelles (eq 3.3). The laponite core is fixed to have a diameter of 25 nm and a thickness of 0.9 nm. From model fitting, we find that the PF127 shell is 1.6 nm thick over both the particle face and edge. The micelles of PF127 are found to have a PPO core of 1.6 nm diameter and a PEO shell of 0.4 nm thickness. With these parameters, we are able to fit the data for both samples at 25°C, the only difference being the particle and micelle volume fractions.

To model the data at 80°C, we will need to also account for clustering of the particles, for which we have included a fractal structure factor<sup>39,40</sup> in addition to the two above form factors. From the model fits at 80°C, we find that the shell of PF127 on the

laponite particles is thicker (5.4 nm over the face, 2.8 nm over the edge). The PF127 micelles are also larger, with a core diameter of 7.6 nm and a shell thickness of 2.2 nm. All the above numbers were used to fit both sets of data. Finally, from the structure factor, we obtain a correlation length, which roughly corresponds to a cluster size: this is 22.4 nm for the non-thermogelling sample and 907 nm for the thermogelling one. A fractal dimension of 2.6, consistent with diffusion-limited aggregation is also found for this case. Important model parameters are listed in Table 4.1. Thus, the modeling confirms clustered particles in the thermogelled sample, and it also indicates larger PF127 micelles and thicker adsorbed layers of PF127 in both samples. Increase of PF127 micelle size with temperature is well-known in the literature and it is believed to occur because the PPO portions of the triblock become more hydrophobic due to dehydration upon heating.

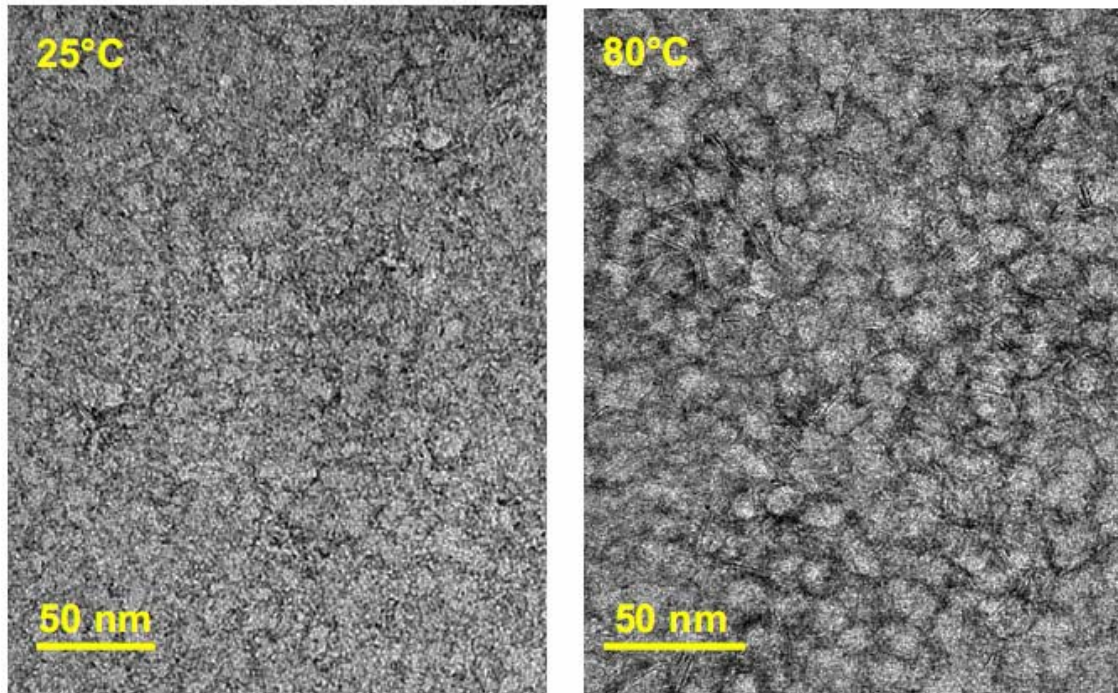


**Figure 4.7.** TEM images corresponding to a 0.5% laponite + 0.6% PF127 sample at 25°C (left) and 80°C (right). The images are stained with uranyl acetate. The image on the right shows a large number of PF127 micelles.

**Thermogelling: TEM Studies.** Further evidence for PF127 micellar growth with temperature is obtained from TEM analysis of our samples. These experiments had to be conducted with a dilute mixture of laponite and PF127 to allow structural details to be resolved. We therefore worked with a sample of 0.5% laponite + 0.6% PF127 and we used uranyl acetate as a negative stain. As described in the Experimental Section, our procedure involved placing a drop of the sample on a TEM grid and drying at either 25°C or 80°C, followed by staining. (During the drying process, the concentrations in solution would increase and possibly fall within the thermogelling range.) The image in Figure 4.7 corresponding to the 80°C sample appears to reveal numerous PF127 micelles of ~ 10 nm

in diameter, which is consistent with the SANS results. In comparison, the image corresponding to the 25°C sample is featureless. It is not possible to resolve individual laponite particles in any of the images, possibly because the disks are less than a nanometer in thickness. The TEM results confirm that relatively large PF127 micelles are present in the sample at high temperature and that these micelles occupy a considerable volume fraction.

**Thermogelling: Mechanism.** There are three possible explanations for thermogelling in laponite/PF127 mixtures. The first is that the laponite particles lose their stabilizing layer of PF127 upon heating, which leads to flocculation. However, it is not clear why the PF127 would desorb from the particles at high temperatures, especially since the increased hydrophobicity of the PPO segment would promote adsorption. Indeed, SANS modeling suggests that the PF127 layer on the particle becomes thicker, not thinner, with heating. Moreover, if thermogelling was due to direct contact between laponite disks, it should be promoted at low PF127 concentrations, but that is not the case (Figure 4.5).

A second possibility is that the laponite disks remain covered with a layer of PF127, but that these surface layers become “sticky” upon heating. Such “stickiness” or attractive interactions between adjacent particles may arise due to the hydrophobicity of the PPO segments at high temperatures. For example, the stickiness may correspond to a bridging interaction between particles. However, bridging is expected to be favored at low PF127 concentrations, which correspond to the particles being incompletely covered<sup>71</sup>. The results, however, show a different trend (Figure 4.5). Also, there is no

evidence that PF127 chains or micelles become sticky (aggregate) upon heating – indeed, large numbers of PF127 micelles co-exist in stable fashion at high temperatures.

A third possibility is that the thermogelling occurs due to *depletion flocculation*., which is an osmotic effect caused by non-interacting polymers. Consider laponite particles stabilized by a layer of PF127. In a thermogelling sample at  $\sim 75^\circ\text{C}$ , the particles will co-exist with a large volume fraction of PF127 micelles having a size of about 10 nm. When the particles approach each other by Brownian motion to a distance less than 10 nm, the micelles will be depleted in the zone between the particles. The higher concentration of micelles in the bulk will then force the particles together, causing flocculation. This is an osmotic effect, and it does not presuppose any direct interaction between the micelles and the particles. The interaction potential is enhanced by having more micelles of sufficient size and the range of the interaction is set by the micelle size. As seen from SANS and TEM, PF127 micelles grow with heating due to the increased hydrophobicity of the PPO segments. Thus, the sample gels at high temperatures because it is only then that the micelles are large enough. The micelles being large is not sufficient; there must also be enough particles such that the average spacing between the particles is not too high. Accordingly, a depletion mechanism can explain a number of key features of the observed thermogelling.

The other crucial experimental fact that can be explained by a depletion-based mechanism is the restabilization observed at higher PF127 loadings. Such an effect is known in the literature and is referred to as *depletion stabilization*<sup>71</sup>. In the present



context, it occurs when the volume fraction of micelles becomes so high that the micelles interfere with the close approach of the particles so as to prevent their flocculation. Note that depletion flocculation of emulsions and particles due to surfactant micelles have been reported in the literature<sup>72</sup>. Depletion stabilization has also been reported in some mixtures of particles and non-adsorbing polymers<sup>73,74</sup> and we believe it is the most reasonable explanation for our results.

#### **4.4. Conclusions**

We have demonstrated thermo-gelling in laponite/PF127 mixtures. At room temperature, PF127 adsorbs onto laponite disks and stabilizes them by steric repulsion. Upon heating, the PF127 layer on the disks becomes thicker, and more importantly, PF127 micelles in the bulk solution grow significantly. At a distinct temperature, the micelles induce *depletion flocculation* of the laponite particles into a gel network. Such thermogelling occurs only if there is sufficient PF127 (and hence its large micelles) as well as a sufficient concentration of the laponite. However, if the PF127 concentration is increased further, the thermogelling is eliminated – this is suggested to be due to the micelles providing *depletion stabilization* of the particles.

## Chapter 5

# Conclusions and Recommendations

---

### 5.1. Conclusions

Responsive complex fluids based on nanostructures (e.g., micelles, vesicles and nanoparticles) have many potential applications, such as sensors, microfluidics or MEMS devices, paints, coatings, and personal care products. However, most of these fluids require molecules made by complex synthesis, which has prevented them from wide use in industry and laboratories. In this dissertation, we have developed new classes of photoresponsive (PR) and thermoresponsive (TR) nanostructures based on commercially available, inexpensive molecules and nanoparticles.

We have developed a new PR fluid based on light-activated nanoparticle assembly, which is reported in Chapter 3. Our system consists of disk-like nanoparticles of laponite along with a surfactant stabilizer (Pluronic F127) and the photoacid generator (PAG), diphenyliodonium-2-carboxylate monohydrate. Initially, the nanoparticles are sterically stabilized by the surfactant and the result is a stable, low-viscosity dispersion. Upon UV irradiation, the PAG gets photolyzed, lowering the pH by about 3 units. In turn, the stabilizing surfactant is displaced from the negatively charged faces of the nanoparticle disks while the edges of the disks become positively charged. The particles are thereby induced to assemble into a 3-dimensional “house-of-cards” network that

extends through the sample volume. The net result is a light-induced *sol to gel transition*, i.e., from a low, water-like viscosity to an *infinite* viscosity and yield stress. The yield stress of the photogel is sufficiently high to support the weight of small objects. The gel can be converted back to a sol by either increasing the pH or the surfactant content. Evidences from a series of experiments along with techniques, including steady and dynamic rheology, small-angle neutron scattering (SANS) are used to illustrate what happened in the system.

In Chapter 4, we have demonstrated a system (laponite + PF127) similar to the photo-gelling nanoparticles dispersion is also a thermo-gelling system. The system has a low viscosity like water at room temperature, but will become a gel at high temperatures like 70°C. The system can revert back to the original viscosity by cooling. The underlying behavior is also laponite nanoparticles self-assembly, but the mechanism for nanoparticles assembly is very different. At room temperature, similar to the photo-gelling system, PF127 stabilizes the laponite dispersion by steric repulsion. At high temperatures, PF127 will form big micelles and fill up the volume. Then the laponite nanoparticles will form clusters due to depletion flocculation. The continuous increase of PF127 size with temperature has led to the abrupt viscosity increase in steady rheology, which has similarity to the pure PF127 thermo-gelling happening at much higher concentration. More PF127 than optimal will lead to no thermo-gelling behavior, which further proves the depletion flocculation mechanism. TEM images are also shown here for further support.

## 5.2. Recommendations for Future Work

The photoacid generator (PAG) we used in Chapter 3 undergoes irreversible dissociation upon UV exposure. If we were to use a photo-reversible PAG, the viscosity changes could be reversed by light irradiation at a different wavelength. However, such a reversible PAG is not commercially available. However, there is a commercially available photobase generator MGC and we have used it to create a new class of PR fluids that show a significant, but reversible drop in viscosity upon UV irradiation. Possible mechanism is related to reverse worm-like micelles length change.

The system is composed of soy lecithin, water, cyclohexane and MGC. Soy lecithin/water/cyclohexane is well known to form reverse worm-like micelles in certain range of water to lecithin ratio<sup>75</sup>. MGC as shown in Figure 5.1 has the following property: upon UV irradiation MGC dissociates, causing an increase in the pH of aqueous solutions, but once UV exposure is stopped, MGC automatically reverts back to its undissociated form<sup>76</sup>.

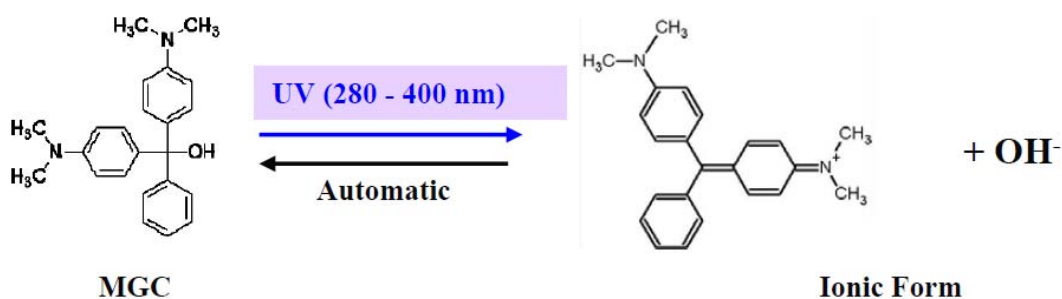


**Figure 5.1.** Photolysis of MGC, a photobase generator (PBG). Upon UV irradiation, the molecule dissociates and releases OH<sup>-</sup>. After UV, it will automatically reverse back.

Figure 5.2 shows UV response of 100mM lecithin+600mM water+0.48mM MGC in cyclohexane. Pictures are taken 1 second after inverting the vials. The sample is initially of gel-like behavior, which flows down very slowly in a 20ml vial, initially even not noticeable, and trap stir bar. Figure 5.2a shows the 20ml vial 1 second after inverting. After 1 minute UV irradiation, the sample shows runny low viscosity. Figure 5.2b shows the irradiated sample in the small vial 1 second after inverting. 10 minutes later, the sample goes back to its original viscosity. Figure 5.2c shows such a sample 1 second after inverting the small vial.

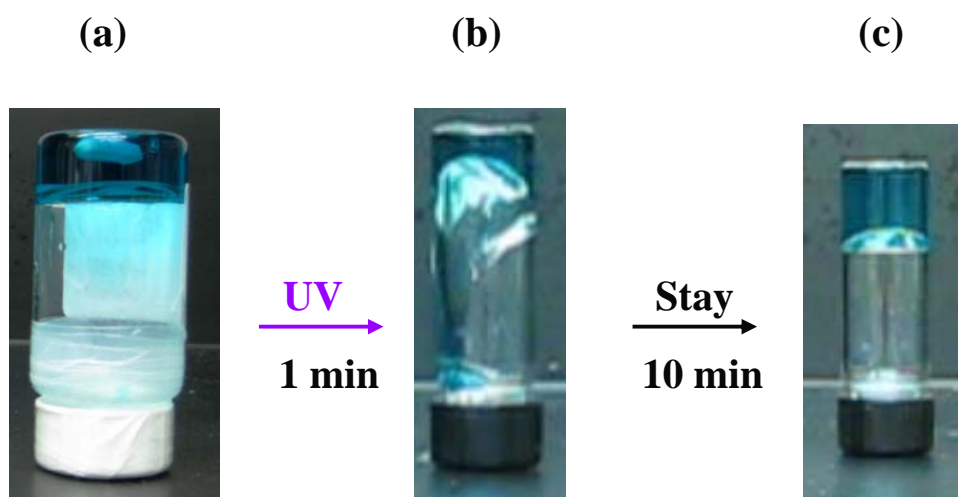


**Figure 5.2.** UV response of 100mM lecithin+600mM water+0.48mM MGC in cyclohexane. Pictures are taken 1 second after inverting the vials.

Due to the reversible nature, rheology data are difficult to be obtained. Current after UV rheology data is significantly lower than the visual observation. More rheology studies about influence of different components in the system and also further investigation into the possible mechanism should be done to make this a complete work.

## References

- [1] Bromberg, L. E.; Ron, E. S. "Temperature-responsive gels and thermogelling polymer matrices for protein and peptide delivery." *Advanced Drug Delivery Reviews* **1998**, *31*, 197-221.
- [2] Hao, T. "Electrorheological fluids." *Advanced Materials* **2001**, *13*, 1847-+.
- [3] Minagawa, K.; Koyama, K. "Electro- and magneto-rheological materials: Stimuli-induced rheological functions." *Current Organic Chemistry* **2005**, *9*, 1643-1663.
- [4] Bossard, F.; Aubry, T.; Gotzamanis, G.; Tsitsilianis, C. "pH-Tunable rheological properties of a telechelic cationic polyelectrolyte reversible hydrogel." *Soft Matter* **2006**, *2*, 510-516.
- [5] Vesperinas, A.; Eastoe, J.; Wyatt, P.; Grillo, I.; Heenan, R. K. "Photosensitive gelatin." *Chemical Communications* **2006**, 4407-4409.
- [6] Lee, C. T.; Smith, K. A.; Hatton, T. A. "Photoreversible viscosity changes and gelation in mixtures of hydrophobically modified polyelectrolytes and photosensitive surfactants." *Macromolecules* **2004**, *37*, 5397-5405.
- [7] Pouliquen, G.; Tribet, C. "Light-triggered association of bovine serum albumin and azobenzene-modified poly(acrylic acid) in dilute and semidilute solutions." *Macromolecules* **2006**, *39*, 373-383.
- [8] Eastoe, J.; Vesperinas, A. "Self-assembly of light-sensitive surfactants." *Soft Matter* **2005**, *1*, 338-347.
- [9] Sakai, H.; Orihara, Y.; Kodashima, H.; Matsumura, A.; Ohkubo, T.; Tsuchiya, K.; Abe, M. "Photoinduced reversible change of fluid viscosity." *Journal of the American Chemical Society* **2005**, *127*, 13454-13455.
- [10] Ketner, A. M.; Kumar, R.; Davies, T. S.; Elder, P. W.; Raghavan, S. R. "A simple class of photorheological fluids: Surfactant solutions with viscosity tunable by light." *Journal of the American Chemical Society* **2007**, *129*, 1553-1559.
- [11] Kumar, R.; Raghavan, S. R. "Photogelling fluids based on light-activated growth of zwitterionic wormlike micelles." *Soft Matter* **2009**, *5*, 797-803.
- [12] Theng, B. K. G. *The chemistry of clay-organic reactions*; John Wiley & Sons: New York - Toronto, 1974.
- [13] Negrete-Herrera, N.; Putaux, J. L.; Bourgeat-Lami, E. "Synthesis of polymer/Laponite nanocomposite latex particles via emulsion polymerization

- using silylated and cation-exchanged Laponite clay platelets." *Progress in Solid State Chemistry* **2006**, *34*, 121-137.
- [14] Cases, J. M. "Zero Charge Point and Silicate Structure." *Journal De Chimie Physique Et De Physico-Chimie Biologique* **1969**, *66*, 1602-&.
- [15] Thompson, D. W.; Butterworth, J. T. "The Nature of Laponite and Its Aqueous Dispersions." *Journal of Colloid and Interface Science* **1992**, *151*, 236-243.
- [16] Dijkstra, M.; Hansen, J. P.; Madden, P. A. "Gelation of a Clay Colloid Suspension." *Physical Review Letters* **1995**, *75*, 2236-2239.
- [17] Nelson, A.; Cosgrove, T. "Small-angle neutron scattering study of adsorbed pluronic tri-block copolymers on laponite." *Langmuir* **2005**, *21*, 9176-9182.
- [18] Baghdadi, H. A.; Sardinha, H.; Bhatia, S. R. "Rheology and gelation kinetics in laponite dispersions containing poly(ethylene oxide)." *Journal of Polymer Science Part B-Polymer Physics* **2005**, *43*, 233-240.
- [19] Gu, H. Y.; Zhang, W. Q.; Feng, K. S.; Neckers, D. C. "Photolysis of ((3-trimethylsilyl)propoxy)phenyl) phenyliodonium salts in the presence of 1-naphthol and 1-methoxynaphthalene." *Journal of Organic Chemistry* **2000**, *65*, 3484-3488.
- [20] Macosko, C. W. *Rheology: Principles, measurements and applications.*; VCH Publishers: New York, 1994.
- [21] Larson, R. G. *The structure and rheology of complex fluids*; Oxford University Press: Oxford, 1999.
- [22] Morrison, F. A. *Understanding rheology*; Oxford University Press: New York, 2001.
- [23] Zemb, T., Lindner, P. *Neutron, X-Ray and Light scattering: Introduction to an investigative tool for colloidal and polymeric systems*; Elsevier: Amsterdam, 1991.
- [24] Brown, W. *Dynamic light scattering: The method and some applications*; Clarendon Press: Oxford, 1993.
- [25] Wolff, T.; Emming, C. S.; Suck, T. A.; Von Bunau, G. "Photorheological Effects in Micellar Solutions Containing Anthracene-Derivatives - a Rheological and Static Low-Angle Light-Scattering Study." *Journal of Physical Chemistry* **1989**, *93*, 4894-4898.
- [26] Wolff, T.; Klausner, B. "Overlap of Colloid Chemistry and Photochemistry in Surfactant Systems." *Advances in Colloid and Interface Science* **1995**, *59*, 31-94.

- [27] Paulusse, J. M. J.; Sijbesma, R. P. "Molecule-based rheology switching." *Angewandte Chemie-International Edition* **2006**, *45*, 2334-2337.
- [28] Yager, K. G.; Barrett, C. J. "Novel photo-switching using azobenzene functional materials." *Journal of Photochemistry and Photobiology a-Chemistry* **2006**, *182*, 250-261.
- [29] Moniruzzaman, M.; Sabey, C. J.; Fernando, G. F. "Photoresponsive polymers: An investigation of their photoinduced temperature changes during photoviscosity measurements." *Polymer* **2007**, *48*, 255-263.
- [30] Pouliquen, G.; Amiel, C.; Tribet, C. "Photoresponsive viscosity and host-guest association in aqueous mixtures of poly-cyclodextrin with azobenzene-modified poly(acrylic)acid." *Journal of Physical Chemistry B* **2007**, *111*, 5587-5595.
- [31] Yagai, S.; Nakajima, T.; Kishikawa, K.; Kohmoto, S.; Karatsu, T.; Kitamura, A. "Hierarchical organization of photoresponsive hydrogen-bonded rosettes." *Journal of the American Chemical Society* **2005**, *127*, 11134-11139.
- [32] Matsumoto, S.; Yamaguchi, S.; Ueno, S.; Komatsu, H.; Ikeda, M.; Ishizuka, K.; Iko, Y.; Tabata, K. V.; Aoki, H.; Ito, S.; Noji, H.; Hamachi, I. "Photo gel-sol/sol-gel transition and its patterning of a supramolecular hydrogel as stimuli-responsive biomaterials." *Chemistry-a European Journal* **2008**, *14*, 3977-3986.
- [33] van Olphen, H. *An Introduction to Clay Colloid Chemistry*; Wiley: New York, 1977.
- [34] Dektar, J. L.; Hacker, N. P. "Photochemistry of diaryliodonium salts." *Journal of Organic Chemistry* **1990**, *55*, 639-647.
- [35] Gu, H. Y.; Ren, K. T.; Grinevich, O.; Malpert, J. H.; Neckers, D. C. "Characterization of iodonium salts differing in the anion." *Journal of Organic Chemistry* **2001**, *66*, 4161-4164.
- [36] Reichmanis, E.; Houlihan, F. M.; Nalamasu, O.; Neenan, T. X. "Chemical amplification mechanisms for microlithography." *Chemistry of Materials* **1991**, *3*, 394-407.
- [37] Scherrer, R. A.; Beatty, H. R. "Preparation of ortho-substituted benzoic acids by the copper(II)-catalyzed reaction of diphenyliodonium-2-carboxylate with anilines and other nucleophiles." *Journal of Organic Chemistry* **1980**, *45*, 2127-2131.
- [38] Rankin, P. J.; Ginder, J. M.; Klingenberg, D. J. "Electro- and magneto-rheology." *Current Opinion in Colloid and Interface Science* **1998**, *3*, 373-381.



- [39] Pedersen, J. S. "Analysis of small-angle scattering data from colloids and polymer solutions: modeling and least-squares fitting." *Advances in Colloid and Interface Science* **1997**, *70*, 171-210.
- [40] Teixeira, J. "Small-angle scattering by fractal systems." *Journal of Applied Crystallography* **1988**, *21*, 781-785.
- [41] Nelson, A.; Cosgrove, T. "A small-angle neutron scattering study of adsorbed poly(ethylene oxide) on laponite." *Langmuir* **2004**, *20*, 2298-2304.
- [42] Wanka, G.; Hoffmann, H.; Ulbricht, W. "Phase-diagrams and aggregation behavior of poly(oxyethylene)-poly(oxypropylene)-poly(oxyethylene) triblock copolymers in aqueous solutions." *Macromolecules* **1994**, *27*, 4145-4159.
- [43] Pignon, F.; Magnin, A.; Piau, J. M.; Cabane, B.; Lindner, P.; Diat, O. "Yield stress thixotropic clay suspension: Investigation of structure by light, neutron, and x-ray scattering." *Physical Review E* **1997**, *56*, 3281-3289.
- [44] Annable, T.; Buscall, R.; Ettelaie, R.; Whittlestone, D. "The rheology of solutions of associating polymers - Comparison of experimental behavior with transient network theory." *Journal of Rheology* **1993**, *37*, 695-726.
- [45] Liao, D.; Dai, S.; Tam, K. C. "Rheological properties of hydrophobic ethoxylated urethane (HEUR) in the presence of methylated beta-cyclodextrin." *Polymer* **2004**, *45*, 8339-8348.
- [46] Liao, D. S.; Dai, S.; Tam, K. C. "Rheological properties of a telechelic associative polymer in the presence of alpha- and methylated beta-cyclodextrins." *Journal of Physical Chemistry B* **2007**, *111*, 371-378.
- [47] Liao, D. S.; Dai, S.; Tam, K. C. "Influence of anionic surfactant on the rheological properties of hydrophobically modified polyethylene-oxide/cyclodextrin inclusion complexes." *Journal of Rheology* **2009**, *53*, 293-308.
- [48] Guenet, J. M. *Thermoreversible Gelation of Polymers and Biopolymers*; Academic Press: London, 1992.
- [49] Croce, V.; Cosgrove, T.; Dreiss, C. A.; King, S.; Maitland, G.; Hughes, T. "Giant micellar worms under shear: A rheological study using SANS." *Langmuir* **2005**, *21*, 6762-6768.
- [50] Croce, V.; Cosgrove, T.; Maitland, G.; Hughes, T.; Karlsson, G. "Rheology, cryogenic transmission electron spectroscopy, and small-angle neutron scattering of highly viscoelastic wormlike micellar solutions." *Langmuir* **2003**, *19*, 8536-8541.

- [51] Glatter, O. "New Method for Evaluation of Small-Angle Scattering Data." *Journal of Applied Crystallography* **1977**, *10*, 415-421.
- [52] Glatter, O.; Fritz, G.; Lindner, H.; Brunner-Popela, J.; Mittelbach, R.; Strey, R.; Egelhaaf, S. U. "Nonionic micelles near the critical point: Micellar growth and attractive interaction." *Langmuir* **2000**, *16*, 8692-8701.
- [53] Yang, H.; Tan, Y. B.; Wang, Y. X. "Fabrication and properties of cucurbit[6]uril induced thermo-responsive supramolecular hydrogels." *Soft Matter* **2009**, *5*, 3511-3516.
- [54] Ramakrishnan, S.; Zukoski, C. F. "Microstructure and rheology of thermoreversible nanoparticle gels." *Langmuir* **2006**, *22*, 7833-7842.
- [55] Jeong, B.; Kibbey, M. R.; Birnbaum, J. C.; Won, Y. Y.; Gutowska, A. "Thermogelling biodegradable polymers with hydrophilic backbones: PEG-g-PLGA." *Macromolecules* **2000**, *33*, 8317-8322.
- [56] Bossard, F.; Tsitsilianis, C.; Yannopoulos, S. N.; Petekidis, G.; Sfika, V. "A novel thermothickening phenomenon exhibited by a triblock polyampholyte in aqueous salt-free solutions." *Macromolecules* **2005**, *38*, 2883-2888.
- [57] Nair, L. S.; Starnes, T.; Ko, J. W. K.; Laurencin, C. T. "Development of injectable thermogelling chitosan-inorganic phosphate solutions for biomedical applications." *Biomacromolecules* **2007**, *8*, 3779-3785.
- [58] Kalur, G. C.; Frounfelker, B. D.; Cipriano, B. H.; Norman, A. I.; Raghavan, S. R. "Viscosity increase with temperature in cationic surfactant solutions due to the growth of wormlike micelles." *Langmuir* **2005**, *21*, 10998-11004.
- [59] Davies, T. S.; Ketner, A. M.; Raghavan, S. R. "Self-assembly of surfactant vesicles that transform into viscoelastic wormlike micelles upon heating." *Journal of the American Chemical Society* **2006**, *128*, 6669-6675.
- [60] Kidowaki, M.; Zhao, C. M.; Kataoka, T.; Ito, K. "Thermoreversible sol-gel transition of an aqueous solution of polyrotaxane composed of highly methylated alpha-cyclodextrin and polyethylene glycol." *Chemical Communications* **2006**, 4102-4103.
- [61] Lambourne, R.; Strivens, T. A. *Paint and Surface Coatings: Theory and Practice*, Second ed.; William Andrew Publishing, 1999.
- [62] Jiang, Z. Q.; Hao, J. Y.; You, Y. J.; Gu, Q.; Cao, W. M.; Deng, X. M. "Biodegradable Thermogelling Hydrogel of P(CL-GL)-PEG-P(CL-GL) Triblock Copolymer: Degradation and Drug Release Behavior." *Journal of Pharmaceutical Sciences* **2009**, *98*, 2603-2610.

- [63] Stoeber, B.; Hu, C. M. J.; Liepmann, D.; Muller, S. J. "Passive flow control in microdevices using thermally responsive polymer solutions." *Physics of Fluids* **2006**, *18*.
- [64] Jiang, Z. Q.; Hao, J. Y.; You, Y. J.; Liu, Y.; Wang, Z. H.; Deng, X. M. "Biodegradable and thermoreversible hydrogels of poly(ethylene glycol)-poly(epsilon-caprolactone-co-glycolide)-poly(ethylene glycol) aqueous solutions." *Journal of Biomedical Materials Research Part A* **2008**, *87A*, 45-51.
- [65] Cleary, J.; Bromberg, L. E.; Magner, E. "Diffusion and release of solutes in pluronic-g-poly(acrylic acid) hydrogels." *Langmuir* **2003**, *19*, 9162-9172.
- [66] Ventzki, R.; Stegemann, J. "High-throughput separation of DNA and proteins by three-dimensional geometry gel electrophoresis: Feasibility studies." *Electrophoresis* **2003**, *24*, 4153-4160.
- [67] Kan, C. W.; Doherty, E. A. S.; Barron, A. E. "A novel thermogelling matrix for microchannel DNA sequencing based on poly-N-alkoxyalkylacrylamide copolymers." *Electrophoresis* **2003**, *24*, 4161-4169.
- [68] <http://www.thermogel.com.au/homeGel.php>.
- [69] Escobar-Chavez, J. J.; Lopez-Cervantes, M.; Naik, A.; Kalia, Y. N.; Quintanar-Guerrero, D.; Ganem-Quintanar, A. "Applications of thermoreversible pluronic F-127 gels in pharmaceutical formulations." *Journal of Pharmacy and Pharmaceutical Sciences* **2006**, *9*, 339-358.
- [70] Jiang, J.; Burger, C.; Li, C. H.; Li, J.; Lin, M. Y.; Colby, R. H.; Rafailovich, M. H.; Sokolov, J. C. "Shear-induced layered structure of polymeric micelles by SANS." *Macromolecules* **2007**, *40*, 4016-4022.
- [71] Hunter, R. J. *Foundations of colloid science* Oxford University Press: Oxford ; New York 2001.
- [72] Tuinier, R.; Rieger, J.; de Kruif, C. G. "Depletion-induced phase separation in colloid-polymer mixtures." *Advances in Colloid and Interface Science* **2003**, *103*, 1-31.
- [73] Ogden, A. L.; Lewis, J. A. "Effect of nonadsorbed polymer on the stability of weakly flocculated suspensions." *Langmuir* **1996**, *12*, 3413-3424.
- [74] Sernenov, A. N. "Theory of colloid stabilization in semidilute polymer solutions." *Macromolecules* **2008**, *41*, 2243-2249.

- [75] Scartazzini, R.; Luisi, P. L. "Organogels from Lecithins." *Journal of Physical Chemistry* **1988**, *92*, 829-833.
- [76] Irie, M. "Light-Induced Reversible Ph Change." *Journal of the American Chemical Society* **1983**, *105*, 2078-2079.